Journal of Structural Geology, Vol. 15, Nos 3–5, pp. 523 to 541, 1993
Printed in Great Britain

0191-8141/93 $06.00+0.00

Kinematic model for the curvature of the northern Subalpine Chain, France

DAVID A. FERRILL* and RICHARD H. GROSHONG, JR

Department of Geology, The University of Alabama, Tuscaloosa, AL 35487-0338, U.S.A.

(*Received* 6 *January* 1992; *accepted in revised form* 31 *July* 1992)

Abstract—Analyses of cross-sectional shortening, mapped faults and calcite twin strain are used in conjunction with geometric–kinematic modeling to interpret the mechanism of curvature formation in the northern Subalpine Chain of France. There is a 45° change in strike around the Chain that is convex towards the foreland (northwest). Five models for fold–thrust belt curvature are applied to the northern Subalpine Chain. They can reproduce the geometry and the kinematic history of a curved fold–thrust belt and can be used to predict the magnitude and orientations of strains and the three-dimensional geometry of the curvature. The models are: pure bending; radial thrusting; curve-parallel simple shear; uniform displacement–uniform shortening; and transport-parallel simple shear. Two principal criteria for distinguishing among the models geometrically are the horizontal tangential strain (extension or contraction parallel to strike) and cross-sectional shortening. The transport-parallel simple shear model predicts no tangential extension in the central domain and greater radial shortening and significant tangential extension in the northeastern and southern domains. This is the pattern observed in the northern Subalpine Chain. Therefore, the curvature of the northern Subalpine Chain is attributed to a transport-parallel simple shear mechanism.

INTRODUCTION

THE northern Subalpine Chain has a 45° change in strike that defines a curvature in map view that is convex towards the foreland. In the present paper, the curvature is analyzed by first quantifying the curvature shape and strains (thin section to cross-section and map scale) and then comparing the measured strains with the strains predicted by various end-member geometric–kinematic models that were derived based on different kinematic assumptions (Ferrill 1991a). The kinematic evolution of the curvature can be interpreted by finding the geometric–kinematic model that best fits the natural curvature and is consistent with the known regional kinematics.

Curvatures in fold–thrust belts around the world have been the subject of study most notably in the western Alps, the Jura, the Iberian Arc (Cantabrian zone, northwestern Spain), the Gibraltar Arc, the Appalachians (several curvatures), the Ouachitas, the Idaho–Wyoming fold–thrust belt in the Rockies, the Carpathians, and the Himalaya and associated Sulaiman and Makran Ranges. Curvatures in these mountain ranges have been explained by various mechanisms or combinations of mechanisms including: changing thrust direction, radial thrusting, basement wrench faulting, impingement on basement obstacles, stratigraphic pinchout of a detachment horizon, change in thickness of the stratigraphic sequence involved in the folding and thrusting, bending of an originally straight belt, welding onto an irregular continental margin, rigid indenter, and reversal of concavity of a down-going plate (Ferrill 1991a).

Curvature analysis is commonly approached using geometric relationships of structural features (e.g. patterns of folds, faults and strain). The geometric relationships of geologic structures are typically compared to qualitative models of curvature development (Laubscher 1972, Matte & Ribeiro 1975, Ries & Shackleton 1976, Marshak 1988). Marshak (1988) emphasized the importance of strain parallel to strike (tangential elongation, either extensional or contractional) for describing a curvature, noting that tangential elongation can be associated with the formation of non-rotational arcs or rotational oroclines. Tangential (strike-parallel) extension or contraction is not typical of nearly straight fold–thrust belts, but is a requirement of many models for fold–thrust belt curvature development (e.g. Matte & Ribeiro 1975, Ries & Shackleton 1976, Merle 1989) and is recognized in several curved fold–thrust belts (Ries & Shackleton 1976, Marshak *et al.* 1982, Marshak 1988, Dietrich 1989).

Five geometric–kinematic models, derived in Ferrill (1991a), are summarized here. The models, given in Fig. 1, are volume constant and can be applied in three dimensions and include models for originally curved fold axes. The emphasis in the present paper will be on the two-dimensional map view, in which the principal features of interest are the curvature shape (change in trend of fold axes), the shortening in cross-section (either perpendicular to strike, parallel to the transport direction, or both) and the strain parallel to the fold axes (tangential elongation).

Critical aspects of the Subalpine Chain structure for hypotheses of curvature formation are the change in trend of the fold axes, spacing of fold axes, strain along regional strike (tangential) and shortening perpendicular to the regional strike. The quantitative kinematic models for curvature development are briefly

*Present address: Shell Offshore Inc., Exploration Department, P.O. Box 61933, New Orleans, LA 70161, U.S.A.

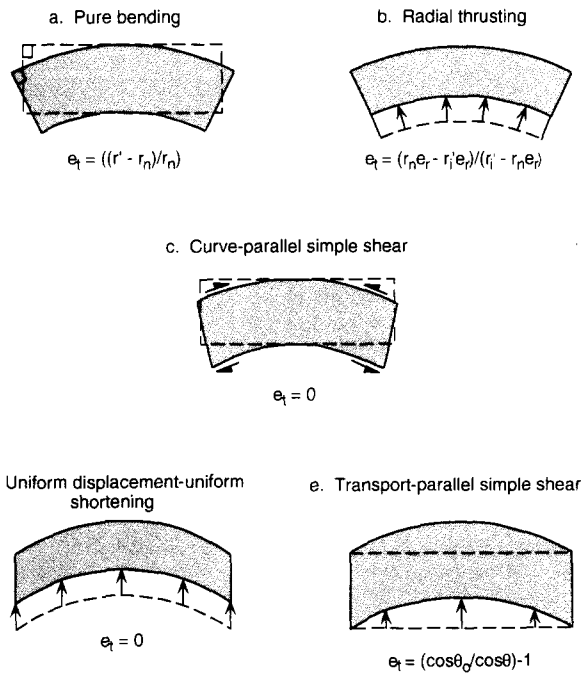

Fig. 1. Five geometric–kinematic models for fold–thrust belt curvature. In the equations; e_t = tangential elongation, r' = radius of any arc with arc length L', r_n = radius of the neutral arc (arc of no length change), r_i' = radius of the inner arc (radial thrusting), e_r = radial shortening, θ = the final angle between the marker line and the transport-normal, and θ_0 = the original angle between the marker line and the transport normal.

reviewed and then applied to the northern Subalpine Chain. New measurements of crystal-plastic strain are presented to test the models.

GEOMETRIC–KINEMATIC MODELS

Pure bending

The pure bending model is defined by a geometry in which all lines that begin perpendicular to the neutral surface remain perpendicular during bending (Fig. 1a). The internal distortion predicted is inner arc contraction and/or outer arc extension (Fig. 1a) in map view. The tangential strain for a curved fold axis in the pure bending model is dependent upon the position of the neutral surface and whether (a) the width of the fold–thrust belt is maintained (tangential plane strain) and vertical thickness changes, or (b) the thickness is maintained while the fold–thrust belt width changes (map view plane strain). A model of tangential plane strain in which the neutral surface is located at the outer arc is characterized by taper towards the foreland which is most consistent with natural fold–thrust belts. The tangential strain predicted by such a model is tangential contraction starting with 0% at the outer arc and increasing towards the inner arc.

Radial thrusting

The radial thrusting model is defined by divergently fanning displacement directions that are perpendicular to strike (Fig. 1b). The outer arc is a surface of zero horizontal strain, because it represents the frontal limit of deformation. The arc of zero horizontal strain is not necessarily fixed but will move towards the foreland (radially) as the fold–thrust belt propagates towards the foreland. The internal distortion predicted in the radial thrusting model is inner arc tangential extension (Fig. 1b) and vertical thickening. Radial displacement of any arc causes stretching after it has formed (Fig. 1b).

Curve-parallel simple shear

The curve-parallel simple shear model (Fig. 1c) has no change in width of the fold–thrust belt that is attributed directly to curvature formation and no tangential extension or contraction. The model is analogous to the flexural folding models of Ramsay (1967). The assumption is made that the fold–thrust belt was initially straight and was subsequently bent. Simple shear parallel to the curve is required due to the constraints of no radial shortening caused by formation of the curvature and no tangential strain.

Uniform displacement–uniform shortening

Fold axes and thrust faults that are initially curved in map view, or folds and thrust faults striking at angles $<90°$ to the transport direction, can form for example because of irregular stratigraphic distribution or control by basement structures. These curved structures are the starting point for the uniform displacement–uniform shortening model (Fig. 1d). The model is defined by uniform displacement magnitude and direction along strike (parallel to the regional transport direction), uniform internal shortening (parallel to the regional transport direction) along strike, and fold axes that do not change their orientation and that experience no tangential extension or contraction. Transpression is expected at the lateral edges of a curvature formed by this mechanism.

Transport-parallel simple shear

The transport-parallel simple shear model is defined by a uniform displacement direction and an along-strike variation in either the displacement magnitude, internal shortening, or both (Figs. 1e and 2) which causes simple shear parallel to the transport direction. The simple shear parallel to the transport direction rotates and extends fold axes that are initially transport-perpendicular and narrows the radial distance between fold axes (Fig. 3). The apparent radial shortening is greater than the actual shortening parallel to the transport direction.

The apparent radial shortening (e_a) between fold axes initiated at some angle θ_0 to the transport normal (having the same sense of structural declination as that caused by the subsequent simple shear) and rotated to some final angle θ is

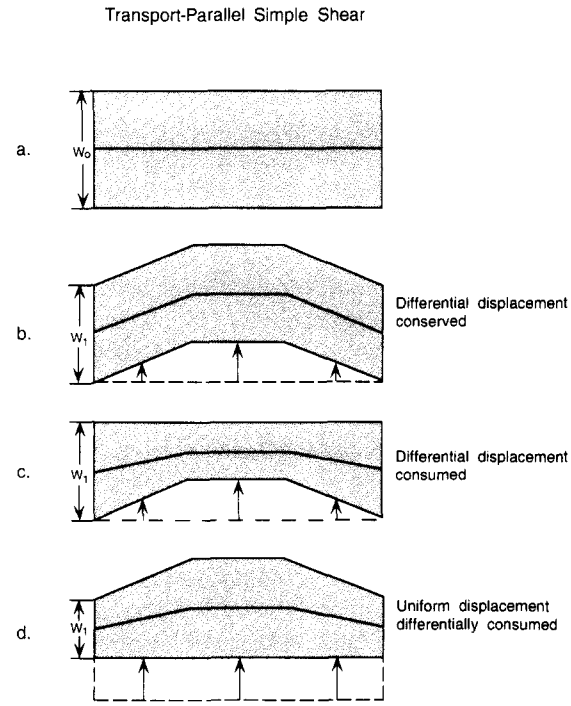

Fig. 2. Three versions of the transport-parallel simple shear model.

$$e_a = \cos\theta/\cos\theta_0 - 1. \quad (1)$$

The rotation and associated strain that results from the differential displacement or differential shortening may be either (a) internally accommodated by small-scale fracturing, faulting and plastic deformation, causing rotation of the map-scale marker lines (Fig. 4b), (b) accommodated by map-scale faulting, causing offset of the map-scale marker lines (Fig. 4d), or (c) a combination of the two mechanisms (Fig. 4c).

The three versions of the transport-parallel simple shear model are: (1) differential displacement conserved (Fig. 2b); (2) differential displacement consumed (Fig. 2c); and (3) uniform displacement differentially consumed (Fig. 2d). The model is volume constant and cross sections parallel to the transport direction are area-constant plane-strain sections. The basic model (differential displacement conserved; Figs. 2b and 3) is defined by uniform transport-parallel shortening along strike and a variation in displacement magnitude along strike. Therefore, in areas of greater displacement, the fold–thrust belt is transported farther towards the foreland. The transport-parallel shortening could occur before or during the curvature development. In the second version of the model (differential displacement consumed; Fig. 2c), the displacement magnitude varies along strike, but the frontal edge is pinned so that the displacement is consumed by horizontal shortening (parallel to the regional transport direction) and vertical thickening. Areas of greater displacement (convex part of the curvature) are, therefore, horizontally shortened and vertically thickened the most. The third version of the model (uniform displacement differentially consumed; Fig. 2d) is defined by uniform displacement magnitude of the trailing edge along strike. The transport-parallel simple

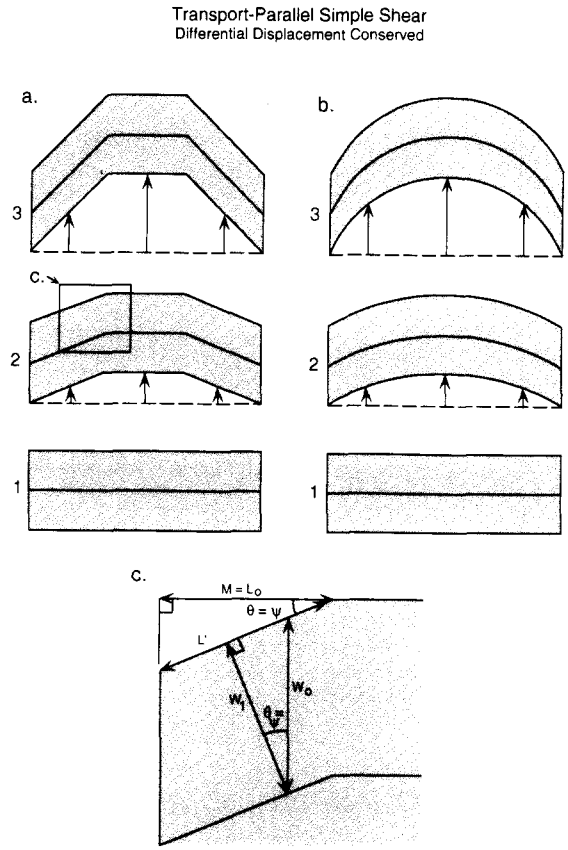

Fig. 3. The transport-parallel simple shear model with different displacement conserved is defined by a uniform displacement direction but non-uniform displacement magnitude. Although differential displacement is conserved, there may be some increment of shortening (e_u) parallel to the transport direction that does not vary along strike. The shape of the curvature is a direct function of the variation of displacement, regardless of the absolute displacement. Simple shear occurs where the displacement varies and causes strike rotation, tangential extension and cross-strike shortening. (a) A linear displacement gradient forms a 'curvature' having domains of constant strike and abrupt changes in strike. (b) A gradual change in displacement forms a smooth curvature. Lengths and angles used in the equations are illustrated in (c).

shear is caused by the along-strike variation in horizontal shortening. The part of a curvature that is convex towards the foreland is shortened and thickened the least.

GEOLOGY OF THE NORTHERN SUBALPINE CHAIN

The northern Subalpine Chain in France is a fold-dominated fold–thrust belt of Mesozoic and Cenozoic sedimentary strata (Fig. 5). The Subalpine Chain is bounded on the foreland (northwest) side by the Molasse basin, containing Cenozoic strata, and on the hinterland (southeast) side by crystalline external basement massifs (Fig. 5). Beyond the Molasse basin to the northwest are the Jura Mountains in which the deformation is thought to generally be younger than in the northern Subalpine Chain (Collet 1927, Laubscher 1972, Burkhard 1990). The northern Subalpine Chain has a cover of far-travelled Ultrahelvetic and Prealpine thrust sheets (Schardt 1898) that were emplaced by the

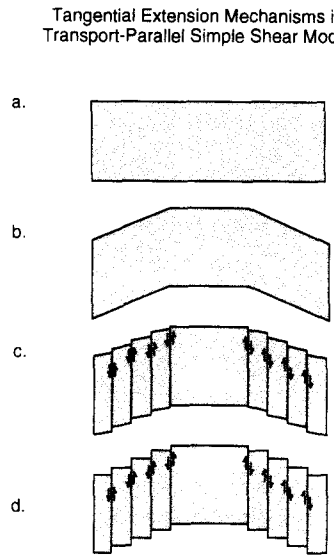

Fig. 4. The tangential extension required by the transport-parallel simple shear model may be accommodated uniformly by thin-section-scale mechanisms and small-scale faulting and extension fracturing (b), by map-scale faulting, here shown as transport-parallel strike-slip faults, and smaller-scale deformation mechanisms (c), or by map-scale faulting alone (d). The initial state is shown in (a).

Pennine thrust (Trümpy 1980, Boyer & Elliott 1982, Ramsay 1989) and carried piggyback by the thrusts of the Subalpine Chain. The thrust at the base of the Ultrahelvetic and Prealpine thrust sheets, the Pennine thrust, has been folded by structures in the Subalpine Chain. The folding in the northern Subalpine Chain has traditionally been thought to post-date the thrusting of the Ultrahelvetic and Prealpine thrust sheets (Schardt 1898, Trümpy 1980, Boyer & Elliott 1982). However, the folding of the Pennine thrust is less than that in the Subalpine Chain beneath (Pairis 1975, Charollais *et al.* 1977, Dunne & Ferrill 1988), which suggests that either the Ultrahelvetic and Prealpine thrust sheets were emplaced during folding in the Subalpine Chain or that the Prealps were detached rather than being folded along with the Subalpine Chain. The rocks of the Pennine thrust have since been eroded leaving klippen of the thrust sheets (Fig. 5).

The frontal part of the northern Subalpine Chain has traditionally been considered to be folded autochthonous or parautochthonous strata in the footwall of the internal part of the sedimentary fold–thrust belt (the Aravis nappe). The Aravis nappe was thought to be the structural equivalent of the Morcles nappe in the Helvetic Alps (Paréjas 1925, Collet 1927). Other workers have stated that the Morcles nappe does not actually correlate across the French–Swiss border and, therefore, is not the structural equivalent of any part of the northern Subalpine Chain (Debelmas & Uselle 1966). Recently, however, specific folds in the frontal part of the northern Subalpine Chain have been correlated with folds in the Morcles nappe (Ramsay 1989). Structural correlation of the root zone of the nappe along strike indicates that both the frontal part of the northern Subalpine Chain and the Aravis nappe belong to the Morcles nappe (Epard 1990).

Uplift of the Aiguilles Rouges massif (Fig. 5) was late and folded the overlying Subalpine Chain (Boyer & Elliott 1982, Pfiffner 1993). A weak SE-dipping reflection has been identified beneath the external basement massifs on the ECORS deep seismic reflection profile (Bayer *et al.* 1987, Guellec *et al.* 1989, Mugnier *et al.* 1990, Nicolas *et al.* 1990). It has been interpreted as the basal décollement, and has been cited as evidence that the external basement massifs were emplaced as brittle thrust sheets, the displacement being transferred towards the foreland beneath the Molasse basin and into the Jura (Bayer *et al.* 1987, Guellec *et al.* 1989, Mugnier *et al.* 1990, Nicolas *et al.* 1990).

A gradual increase in metamorphism from northwest to southeast across the northern Subalpine Chain is illustrated by increased vitrinite reflectance (Kübler *et al.* 1979), increased illite crystallinity (Kübler *et al.* 1979, Aprahamian & Pairis 1981) and higher grade mineral assemblages (Kübler *et al.* 1974, 1979). The increase in metamorphic grade extends from low temperature diagenesis at the front of the belt to anchimetamorphism in the internal part of the belt. The original depth of stratigraphic burial for the uppermost Tertiary stratum is thought to have been less than 1 km, precluding metamorphism due to simple stratigraphic burial (Kübler *et al.* 1974). Metamorphism is thought mainly to result from tectonic burial by the Prealpine nappes that are now only preserved in klippen (Kübler *et al.* 1974). There is a general decrease in metamorphism along strike within the northern Subalpine Chain from northeast to southwest (Ferrill 1991b), which suggests that the overlying Ultrahelvetic and Prealpine thrust sheets were thinner to the southwest due either to less original thickness or to early erosion.

The dominant cliff-forming unit in the northern Subalpine Chain is the approximately 200 m thick Cretaceous Urgonian Limestone (Fig. 6) (Collet 1927, Charollais *et al.* 1977). Figure 6 is a stratigraphic section for the northern part of the study area, which includes the Jurassic and Triassic rocks that are generally not exposed in the central and southern parts of the study area. The mechanical behavior (stiff vs soft) of the stratigraphy is based on field observations and published cross-sections (Pairis 1975, Charollais *et al.* 1977, Epard 1990, Pfiffner 1993). Stiff units tend to maintain their thickness, whereas soft units tend to change thickness and contain décollement horizons. In the northern Subalpine Chain, the dominant stiff members are the Urgonian and upper Jurassic Limestones, the major thrust detachment is in the Aalenian Shale, and another décollement is in the lowermost Cretaceous shales (Epard 1990). Sampling for strain analysis was restricted to the Urgonian Limestone, with the exception of one sample (86-5) from the underlying Hauterivian and two samples of Eocene limestone (85-1 and 86-6). The curvature analysis will concentrate on the exposed Mesozoic stratigraphy and the Urgonian Limestone in particular.

The northern Subalpine Chain is here divided into three strike domains (Fig. 7) for the purpose of characterizing the differences of the structure and strain in

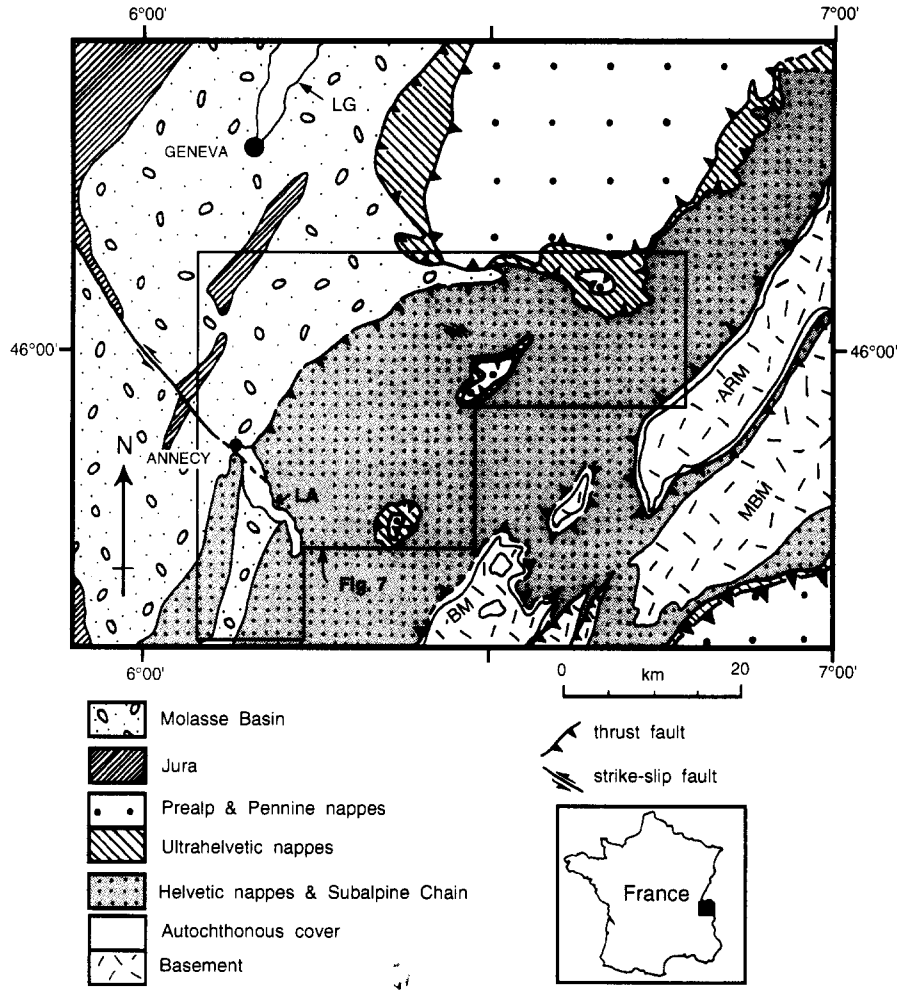

Fig. 5. Location map of the northern Subalpine Chain with regional tectonic elements shown (after Spicher 1980). LA = Lake Annecy, LG = Lake Geneva, ARM = Aiguilles Rouges Massif, MBM = Mont Blanc Massif, BM = Belledone Massif.

different parts of the chain. The central domain has a general strike to the northeast (045°), perpendicular to the assumed regional transport direction (Laubscher 1972, Pijolat *et al.* 1981, Vialon *et al.* 1984, 1989, Choukroune *et al.* 1986, Platt *et al.* 1989, Ramsay 1989, Burkhard 1990, Auborg *et al.* 1991, Gehring *et al.* 1991, Huggenberger & Wildi 1991). To the northeast is a domain with a general strike of 064°, and to the south a domain with folds trending 011°. One cross-section from each domain is illustrated in Fig. 8. Two of the cross-sections (Figs. 8b & c) are new and were constructed using published geologic maps (Goguel 1966, Ricour *et al.* 1969, Charollais 1986). The other cross-section (Fig. 8a) is based on the surface data in cross-sections of Pairis (1975) and Welbon (1988a). The position of basement in the cross-sections is based on the published interpretation of a seismic line through the frontal part of the northern Subalpine Chain and the Molasse basin, a well through the Molasse basin that extends into the Mesozoic strata (Charollais *et al.* 1977), and the ECORS seismic line and published interpretations of the line (Bayer *et al.* 1987, Guellec *et al.* 1989, Mugnier *et al.* 1990, Nicolas *et al.* 1990). A single thickness of the Mesozoic sequence extends beneath the Molasse basin between the Jura and the northern Subalpine Chain. This single thickness of the Mesozoic sequence is projected beneath the Subalpine Chain in Fig. 8. In cross-section, the thin-skinned part of the belt (i.e. above basement) does not have a pronounced taper towards the foreland, but instead appears as a thickened slab and actually thickens towards the foreland (Fig. 8).

Folds and faults

The exposed part of the northern Subalpine Chain fold–thrust belt is fold dominated and lacks major emergent thrust faults cutting the Urgonian Limestone, except for a major thrust around the frontal edge of the belt (Fig. 5) and several smaller-displacement thrust faults in the northeastern domain, along the Arve River (Fig. 8a). Several folds in the belt are detached from the stratigraphic units above and/or below. The isoclinal syncline near the front of cross-section C–C″, based on its tightness, must be detached from the overlying strata. The eroded Urgonian Limestone in Fig. 8(c) was reconstructed from the geology exposed 5 km northeast of the cross-section line and projected parallel to the fold plunge. The Urgonian Limestone is repeated beneath the isoclinal syncline (Fig. 8c), indicating the presence of

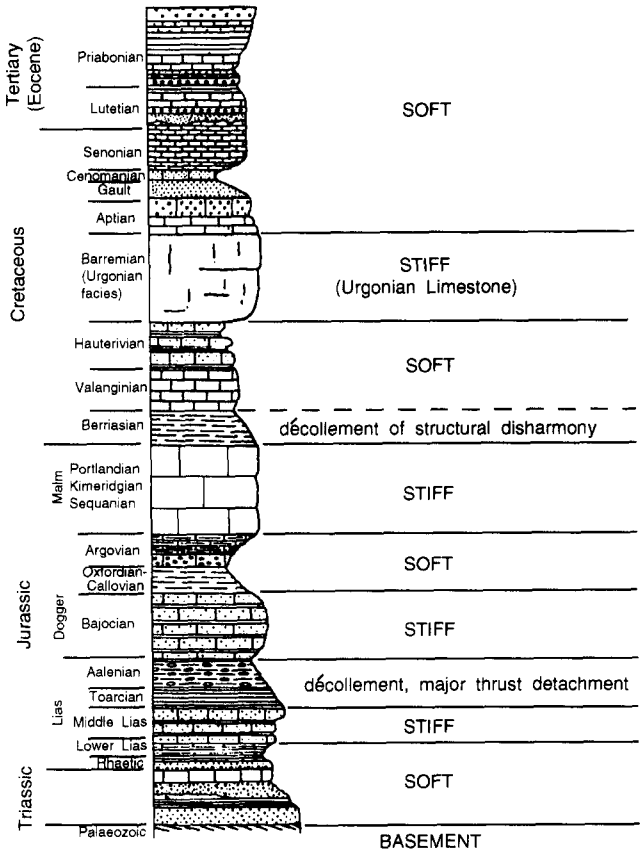

Fig. 6. Stratigraphic section for the area north of the Arve river, and south of the Rhone river (from Collet 1927). The mechanical behavior of the strata (stiff vs soft) is based on field observations and published cross-sections (Pairis 1975, Charollais *et al.* 1977, Epard 1990). Stiff units tend to maintain their thickness and soft units tend to change thickness and contain décollement horizons.

a thrust fault (Charollais *et al.* 1977). In cross-section A–A″ (Fig. 8a), the frontal anticline is too tight to contain the lower stratigraphic units in the core and must be detached from the Mesozoic strata beneath. Thus a thrust fault has been mapped below the anticline (Charollais *et al.* 1977). The exposed Urgonian Limestone in each cross-section is within a single major thrust sheet. Curved-bed shortening for the Urgonian Limestone (measured by comparing the curved-bed lengths and deformed-bed lengths) in the upper panel of each strike-perpendicular (radial) cross-section was measured internal to the hinge of the frontal fold in each section for comparison along strike. Curved-bed shortening varies around the chain from 22% in the northeastern domain (Fig. 8a), to 14% in the central domain (Fig. 8b), and 25% in the southern domain (Fig. 8c).

The large space beneath the Urgonian Limestone and above the crystalline basement, a vertical distance of 5 km or more, is filled with Mesozoic (Charollais *et al.* 1977, Guellec *et al.* 1989, Nicolas *et al.* 1990, Zoetemeijer & Sassi 1992) and possibly Tertiary (Butler *et al.* 1987, Coward & Dietrich 1989) strata. Seismic reflection data have been interpreted to show at least two thrust faults beneath the exposed thrust sheet, filling the space between the exposed thrust sheet and basement with Mesozoic strata (about 2.5 km thick) (Charollais *et al.* 1977, Nicolas *et al.* 1990). The Brizon well, drilled near the front of the fold–thrust belt in the northeastern domain, encountered Mesozoic strata of Cretaceous, Jurassic and Triassic age, and no Tertiary strata beneath the Urgonian Limestone (Huggenberger & Wildi 1991).

The history of fault activity in the northern Subalpine Chain is complicated. Some of the faults are synsedimentary normal faults that were active during the Cretaceous and Tertiary Periods and later reactivated as thrust faults or passively deformed (Pairis 1975, Welbon 1988a,b). Many of the faults post-date at least the initial folding in the northern Subalpine Chain (Doudoux 1973, Pairis & Pairis 1978). Faults that cut across strike are abundant in the study area (Fig. 9) (Goguel 1966, Ricour *et al.* 1969, Charollais 1986). The mean orientations for mapped cross-strike faults that cut the Urgonian Limestone in each domain are as follows (Fig. 10): (a) northeastern domain, 324° ± 20°; (b) central domain, 312° ± 20°; and (c) southern domain, 281° ± 33°. Because of the orientations of the cross-strike faults with respect to strike, either strike-slip or normal displacement will cause strike-parallel extension. Many of the faults in the northeastern and southern domains have mapped strike separations with the correct sense of separation to extend beds parallel to strike (e.g. Fig. 9b) (Huggenberger & Wildi 1991).

In the northeastern domain, fault intensities (measured as faults km^{-1}) along two different belts of Urgonian Limestone outcrops parallel to the fold axes are 1.9 and 4.6 faults km^{-1} along strike (1:50,000 scale geologic map; Charollais 1986). The most conspicuous of the cross-strike faults is a right-lateral strike-separation fault, striking 295° (Fig. 9b), that offsets an anticline trending 060°. The fault has a strike separation of 600 m, which extends the fold along its axis by 340 m. In general, the faults have strike separations of 50 m or less.

A major feature of the southern domain is a strike-slip fault (the Vuache fault) with a trend of 308° that extends from the southeastern part of the Jura across the Molasse basin (Laubscher 1972) and projects into the lake at Annecy (Fig. 5) (Moret 1934, Pierce 1966, Bonnet 1983, Vialon *et al.* 1984). Fold axes apparently correlate across the Annecy valley (Moret 1934, Charollais *et al.* 1977), but they are offset or deflected by the fault or shear zone (Pierce 1966, Laubscher 1972). If these folds, which trend 011°, formed before the strike-slip movement occurred, then they have since been offset approximately 1.9 km (which extends the fold along its axis by 1.06 km) with a left-lateral sense. The displacement diminishes towards the foreland to 1.06 km where the fault offsets the Grand Saleve anticline. The fault continues towards the foreland to form a lateral ramp for a Jura anticline (Fig. 5). The fact that the fault appears to have been active during the latest phase of structural development that formed the Jura Mountains, indicates that strike-slip faulting was active late in the structural evolution of the Subalpine Chain.

The published map for the southern domain (at 1:80,000 scale; Goguel 1966) is less detailed than the map for the central and northeastern domains (at

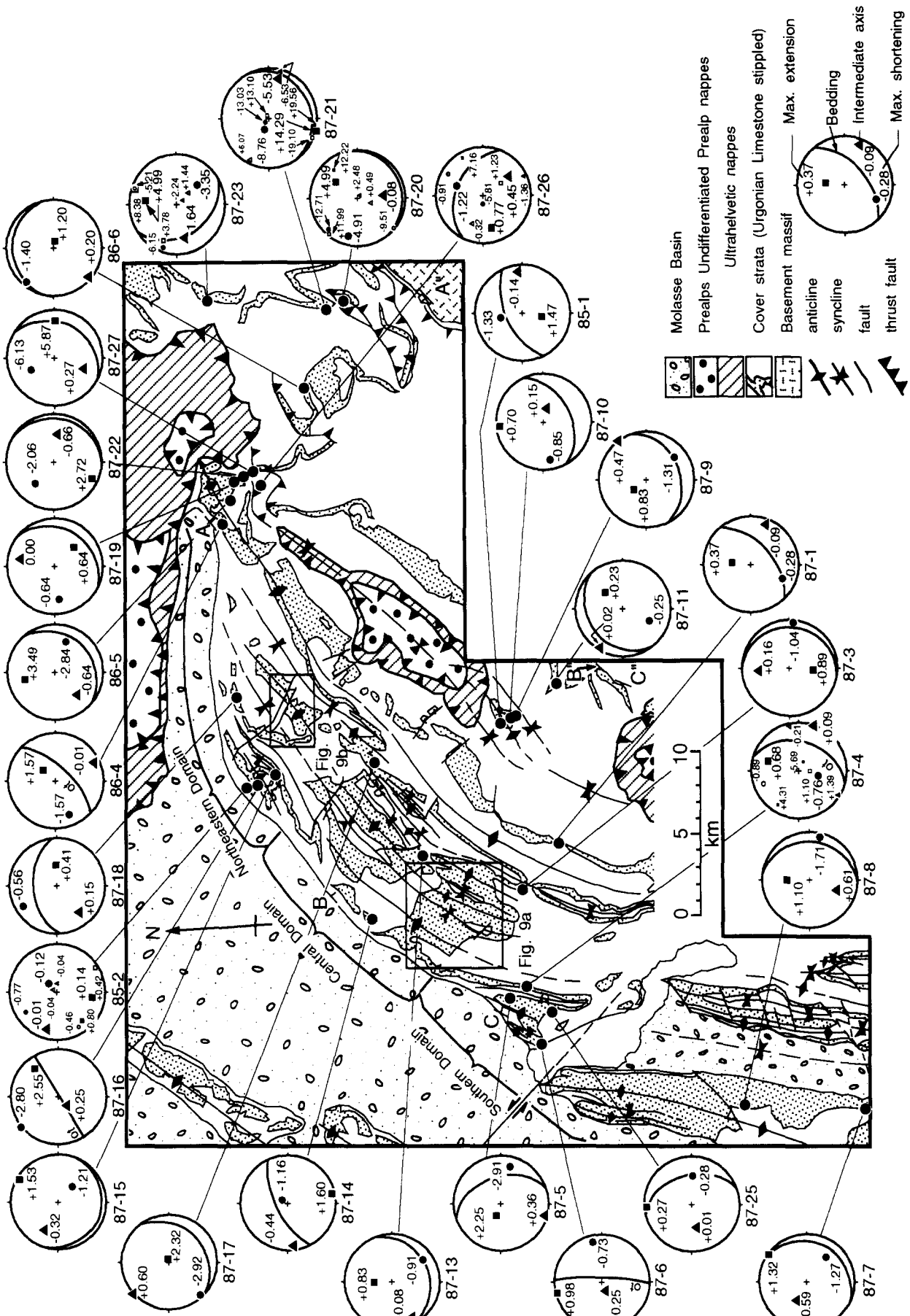

Fig. 7. Map of the northern Subalpine Chain, France, showing locations for samples of Urgonian Limestone, Hauterivian Limestone (86-5) and Eocene Limestone (85-1 and 86-6). Geology is from Ricour *et al.* (1969) and Goguel (1966). Equal-angle projections of the trace of bedding (great circle; ot signifies overturned bedding) and principal strain axes from the calcite strain gauge analysis in the present study, with numbers representing the principal strains in % (− = contraction, + = extension). On stereoplots with multiple sets of symbols; large solid symbols = LDR data, small solid symbols = PEV data, small unfilled symbols = NEV data.

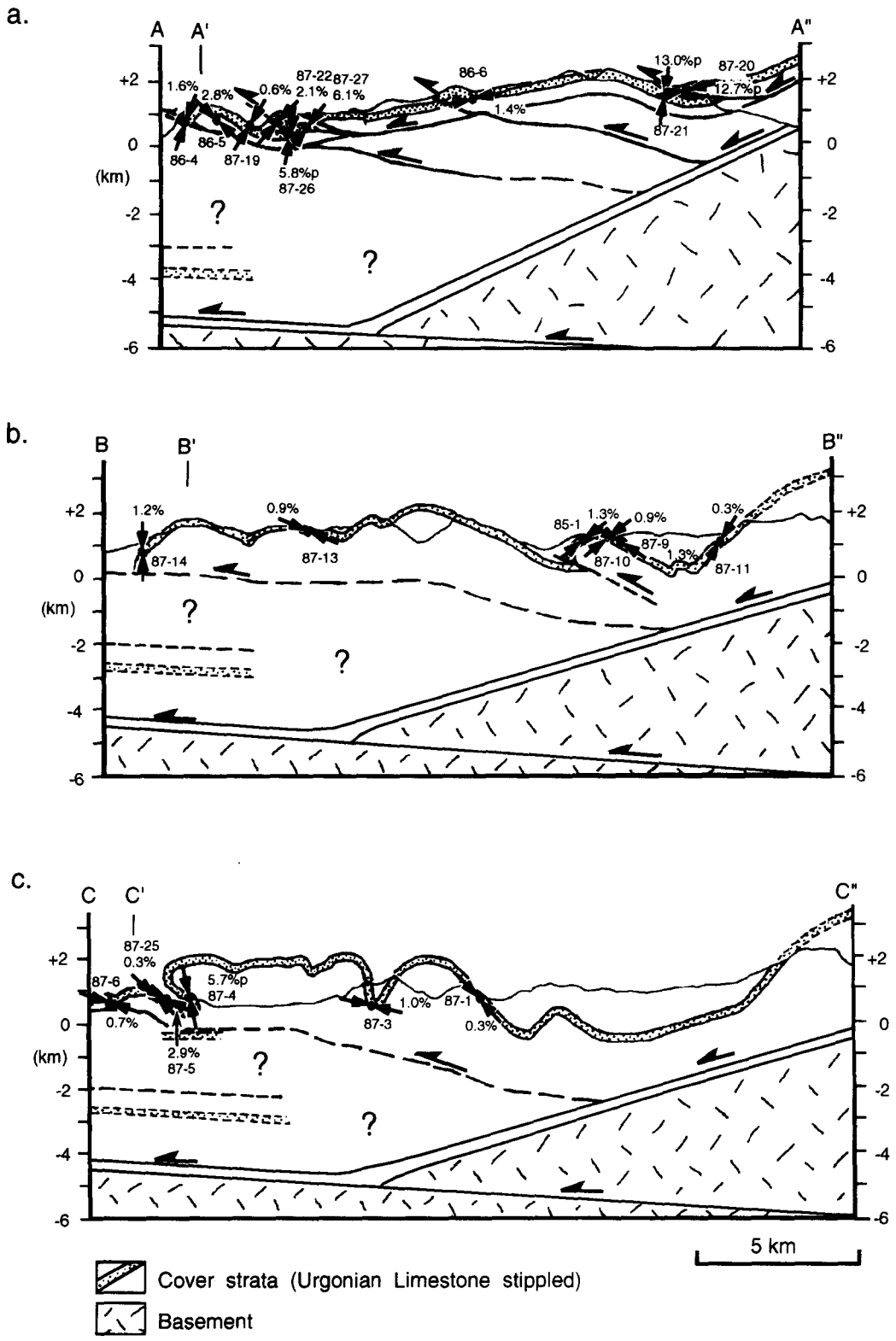

Fig. 8. Cross-sections across the northern Subalpine Chain. Locations of the cross sections are shown in Fig. 7. Curved-bed shortening values for the Urgonian Limestone were measured between the hinge of the frontal anticline and the internal edge in the upper panel in each cross-section. (a) Curved-bed shortening along A′–A″ in the northeastern domain is 22%. (b) Curved-bed shortening along B′–B″ in the central domain is 14%. (c) Curved-bed shortening along C′–C″ in the southern domain is 25%. Values of maximum shortening calcite-twin strain (e_3) at selected locations are shown beside arrows giving direction of maximum shortening and sample number.

1:50,000 scale; Charollais 1986). Along-strike fault intensities for mapped faults in the southern domain, on the 1:80,000 scale map (Goguel 1966), are in the range of 0.36–0.53 faults km^{-1} (average = 0.45 faults km^{-1}). Many of these faults have map-view strike separations that extend the folds along their axes by about 100 m per fault. The central domain has been mapped at two scales, leading to significantly different average fault intensities along the same marker lines: 0.41 faults km^{-1} on the 1:80,000 scale map (Ricour *et al.* 1969) vs 2.0

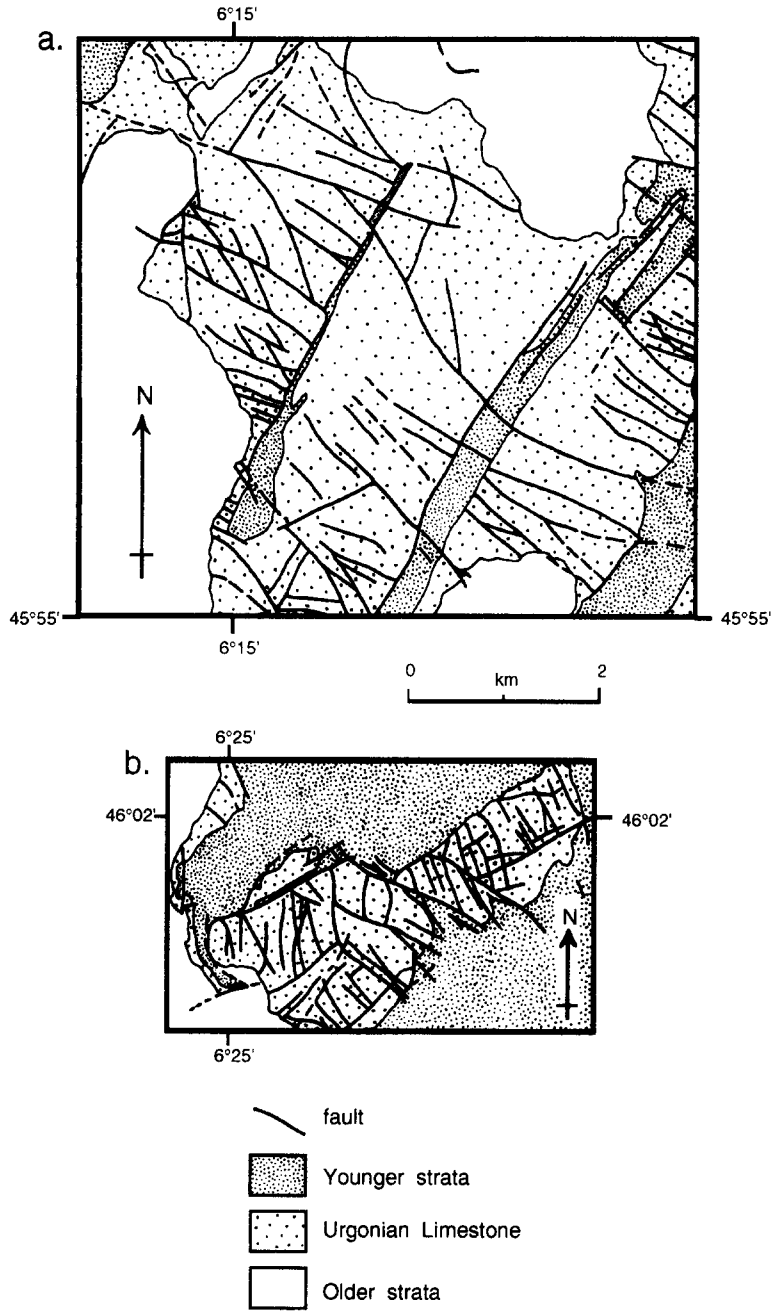

Fig. 9. Maps of representative cross-strike faults (from Charollais 1986) in the central and northeastern strike domains. The locations of these maps are shown in Fig. 7.

faults km^{-1} on the 1:50,000 scale map (Charollais 1986). The 1:80,000 maps for the central and southern domains (Goguel 1966, Ricour *et al.* 1969) illustrate similar intensities for cross-strike faults, of 0.41 and 0.45 faults km^{-1}, respectively, suggesting that the cross-strike fault spacing is similar in the central and southern domains. In the later modeling section, it will be assumed that the southern domain has an average fault intensity similar to that of the central zone on the 1:50,000 scale map (2.0 faults km^{-1}).

Microstructures

Limestone samples collected for microstructural analysis are grainstone and packstone of the Cretaceous Urgonian Limestone, the underlying Hauterivian Limestone and Eocene limestone. The samples contain pelloids and fossils, including echinoderm fragments and foraminifera, matrix and cement. The samples were collected from domains of relatively planar dip so as to avoid the local deformation in small-scale structures or adjacent to faults.

Transgranular stylolites and extension veins are common in thin section. The stylolites are mostly parallel or oblique to bedding at a low to moderate angle and most commonly strike parallel to the strike of bedding. The extension veins are mostly perpendicular to or oblique at a high angle to bedding and most commonly strike perpendicular to the strike of bedding, but they also commonly strike parallel to the strike of bedding. Transgranular microfaults are rare and only appear in thin sections from one sample (87-17).

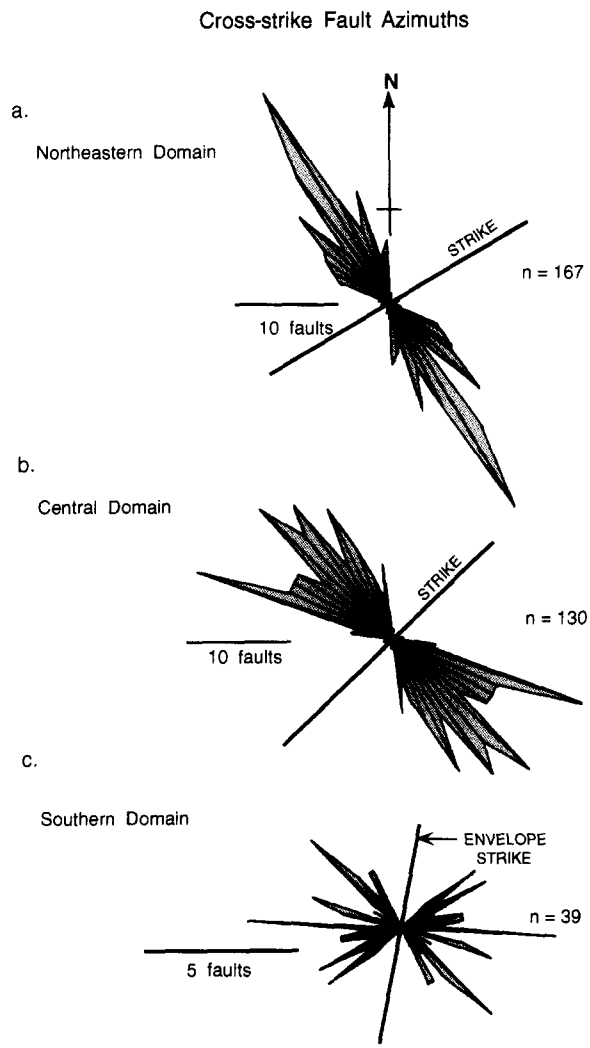

Fig. 10. Rose diagrams of fault azimuths in each strike domain. Fault orientations for the northeastern and central domains were measured from the map of Charollais (1986) and for the southern domain from the map of Goguel (1966).

The only microstructures consistently observed in all thin sections are calcite *e*-twins. Calcite-*e*-twins are the result of geological deformation rather than a product of the thin-sectioning process or an inherent feature of the original rock (Groshong *et al.* 1984a). The twins in the samples for the present study are mostly thin twins, which appear as dark lines in thin section. Thick twins, for which twinned material is visible, are present in some samples and tend to have greater width and relatively low twin intensities (twin intensity = number of twins per mm) in samples of higher metamorphic grade (diagenesis zone 4 and anchizone; Ferrill 1991b). The change in twin width across strike correlates with increasing grade of metamorphism, indicating that the twinning occurred during metamorphism (Ferrill 1991b).

Calcite twinning strain

The strain by calcite twinning is measured using the strain-gauge technique (Groshong 1972, 1974). Experimental tests (Groshong *et al.* 1984b) and comparisons of strain calculated by the calcite strain gauge with bulk strains from finite strain analysis of naturally deformed limestones from the Virginia Appalachians (Evans & Dunne 1991) have demonstrated that the strain gauge gives an accurate measurement of the orientations of the principal strain axes. The calcite twinning strain also accurately represents the magnitude of intragranular strain at low temperatures (Groshong *et al.* 1984b, Evans & Dunne 1991). With increasing temperature an abrupt transition occurs, beyond which other intra- and intergranular mechanisms (e.g. dislocation creep, lattice and grain-boundary diffusion, grain boundary sliding, recrystallization) become operative and accommodate most of the strain (Groshong *et al.* 1984a, Mosar 1988, Evans & Dunne 1991). Groshong *et al.* (1984a) found that in the Helvetic Alps of eastern Switzerland, twinning was the most important intragranular mechanism at or below conditions represented by a mean vitrinite reflectance (R_o) of 3.5 (around 270°C; Groshong *et al.* 1984a). Mosar (1989) found that the strains measured using the calcite strain gauge and bulk strains measured using deformed pellets as markers were about the same in the Prealps Medianes Plastiques, where the metamorphism is in the diagenesis zone and anchizone. In the Prealps Medianes Rigides, where the metamorphism is greater (anchizone and epizone), the strain by calcite twinning is significantly less than the bulk strain recorded by the deformed pellets (Mosar 1989). Evans & Dunne (1991) found that in limestones of the North Mountain thrust sheet of northern Virginia, twinning accommodated virtually all of the intragranular strain and more than half of the finite strain in the semi-brittle non-tectonites (Association III of Groshong 1988), where crystal-plastic strains (e.g. calcite twinning) are in the range of 2–15%, deformed at 250–350°C. The balance of the finite strain was by pressure solution.

The limestones of the northern Subalpine Chain are (with exception of sample 87-21, which is an association IV tectonite) brittle and semi-brittle non-tectonites of deformation mechanism associations II and III (Groshong 1988) and were deformed at low temperatures (55–250°C; Ferrill 1991b, Ferrill & Groshong in press). Because of the low temperatures during deformation, the twinning strain should be representative of the intragranular strain in magnitude and orientation.

Twins were measured in cement and fossil grains (echinoderm fragments where present), exclusively, with the exception of one sample (87-25) where measurements were made using a vein in one thin section because of the scarcity of suitable grains in the rest of the section. Thirty twin sets were measured in each of two mutually perpendicular and bedding-perpendicular thin sections per sample, one cut parallel to strike and the other parallel to dip. Two cleaning strategies were used to improve the precision and accuracy of the results. In the first, the largest-deviations-removed procedure (LDR), the 20% of grains having the largest deviations from the calculated strain tensor were eliminated to clean each sample of the most inhomogeneously deformed grains and the greatest measurement errors (Groshong 1974, Groshong *et al.* 1984b).

This is the standard cleaning procedure. The % negative expected values (% NEV) is the percentage of twin sets in a data set that have the opposite sense of shear to that expected for the computed strain tensor (Groshong 1972). A second cleaning procedure was used in addition to the first for those samples in which one-third or more of the twin sets had negative expected values after the first cleaning. These samples were, in addition to the LDR procedure, processed by separating the original data set (all 60 twin sets) into two subsets; the negative expected values (NEV) and the positive expected values (PEV). The strain gauge was run on the separated subsets, which were then cleaned by removing the one to three twin sets (less than 7% of the sets) with the largest deviations. Some negative expected values typically remain in the NEV and PEV data sets after cleaning and performing the strain gauge calculation.

The three-dimensional strain magnitudes and orientations are shown in Fig. 7 (+=extension and − = contraction). The principal contractions by calcite twinning (LDR data) are −0.13 to −8.76% (Table 1). The principal extensions are +0.14% to +14.29% (LDR data). Principal contractions from PEV calculations are as large as −13.03%, and extensions are as large as +19.56%.

Negative expected values for LDR twin strains in naturally deformed samples are commonly in the range of 10–20% or more (Groshong 1975, Groshong *et al.* 1984a, Spang & Groshong 1981, Mosar 1989, Evans & Dunne 1991) and >40% negative expected values implies multiple deformations or inhomogeneous deformation (Teufel 1980, Groshong *et al.* 1984b). The % negative expected values for the LDR calculations for all of the samples from the northern Subalpine Chain range from 2.08 to 39.58% and average 20.00%. Small % negative expected values indicates homogeneous, coaxial strain. The six samples that have >33% negative expected values for the LDR calculations are from the northeastern (five samples) and southern (one sample) domains. These six samples have probably experienced inhomogeneous or non-coaxial strain.

Near layer-parallel shortening strains perpendicular to fold axes are consistent with twinning before folding, during near layer-parallel shortening, or during buckle folding (Dieterich 1969, Dieterich & Carter 1969, Groshong *et al.* 1984a). Shortening strain axes plunging in the transport direction, commonly at 45° or more, are compatible with compression in a zone of simple shear with the top moving in the transport direction (Sanderson 1982). This sense of shear is appropriate for twinning during translation of a thrust sheet (Sanderson 1982).

The twin strain axes in the northern Subalpine Chain, as a group, do not have uniform bearing and plunge that would indicate that the twinning post-dated folding and curvature development. Twenty-five of the 29 samples have twin strains consistent with, but not necessarily limited to, twinning during folding. In most samples the principal shortening direction is at a low to moderate angle to bedding and plunges in the dip direction. Of these 25 samples, only seven have strain orientations that are exclusively consistent with a syn-folding origin, 11 have orientations consistent with pre- or syn-folding origin, four have orientations that are consistent with a syn- or post-folding origin, and three samples have shallowly dipping to horizontal bedding (0–11°) and strain axis orientations that are equally consistent with a pre-, syn- or post-folding origin (Ferrill 1991a). The principal extension direction in two samples from the upper half of the Urgonian Limestone in the outer arcs of anticlines (87-19 and 87-27) is in the dip direction, indicating outer-arc extension during folding.

Twinning extension parallel to strike is recorded in 23 of the 29 samples. Five of the six samples that lack twinning extension parallel to strike are from the central domain, indicating that little or no crystal-plastic tangential extension occurred in the central domain. The other sample that does not record strike extension by twinning is from the northeastern domain, from the overturned forelimb of the Cluse (Bargy) anticline, at the front of the fold–thrust belt. The averaged tangential elongation for each domain is: southern domain =+0.9%; central domain =−0.2% (contractional); external part of northeastern domain (diagenesis zone 2 and 3 samples; Fig. 7, Table 1) = +1.6%; and internal part of northeastern domain (diagenesis zone 4 and anchizone samples; Fig. 7, Table 1) = +7.6% (LDR) or +12.8% (PEV).

The strain geometry indicates that twin strain axes for most of the Subalpine Chain samples record strains from before or during folding. The map-view curvature of the fold axes in the belt formed either during folding, by rotation or the formation of originally curved fold axes, or after the folding. Therefore, the twin strain axes must record either strains produced during curvature formation or strains produced before curvature development but (potentially) modified by late curvature formation.

CURVATURE DEVELOPMENT

Different models for the development of the curvature of the northern Subalpine Chain have different and predictable consequences for the strain along and across the curvature. Important geologic characteristics that must be accounted for are: (1) the 45° change in strike from northeast to southwest; (2) the different percentages of curved-bed shortening in strike-perpendicular cross sections through the three strike domains (22, 14 and 25%); (3) the difference in the magnitude of tangential elongation by calcite twinning in limestone from the three domains (extensional in the southern and northeastern domains and approximately zero in the central domain); (4) the cross-strike faults that accommodate strike extension, especially in the northeastern and southern domains; and (5) the interpreted regional transport direction (northwestward). Because of the concentration of data for the exposed thrust sheet, and the uncertainty over whether the volume between the exposed thrust sheet and the basement is filled with Mesozoic stratigraphy, Tertiary molasse, or both, the

Table 1. Calcite twin strain data: CP = cleaning procedure (LDR = largest deviations removed, PEV = positive expected values, NEV = negative expected values); twin sets rem. = number of twin sets removed in the cleaning; twin sets = number of sets remaining after cleaning; principal strains (e_1, e_2 and e_3) are measured in % elongation (+ = extension, and − = contraction); nev = negative expected values (%) remaining after calculation; error = nominal error (%) for the twin strain values; zone = metamorphic zone (after Kübler *et al.* 1979); DZ-2–DZ-4 are diagenesis zones 2–4 and AZ-5 is anchizone; bedding = bedding orientation; strain orientations = trend and plunge of principal strains; e_3 to bedding is the angle between the principal shortening axis and the plane of bedding measured in degrees

	Location					Principal strains							Strain orientations			
Sample	Latitude	Longitude	CP	Twin sets rem.	Twin sets	e_1	e_2	e_3	nev	Error	Zone	Bedding	e_1	e_2	e_3	e_3 to bedding
85-1	45°54′55″	6°25′08″	LDR	12	48	1.47	−0.14	−1.33	2.08	0.13	DZ-3	065/5NW	190/47	083/09	348/40	10
85-2	46°03′11″	6°22′33″	LDR	12	48	0.14	−0.01	−0.12	39.58	0.08	DZ-2	000/00	191/19	286/14	047/65	65
			PEV	1	29	0.80	−0.04	−0.77	3.45	0.10	DZ-2	000/00	231/15	093/70	328/14	14
			NEV	1	29	0.42	0.04	−0.46	6.90	0.06	DZ-2	000/00	147/06	019/77	238/10	10
86-4	46°03′35″	6°35′09″	LDR	12	48	1.57	−0.01	−1.57	27.08	0.27	DZ-2	044/66SEO	046/62	155/11	249/26	44
86-5	46°02′56″	6°35′59″	LDR	12	48	3.49	−0.64	−2.84	14.58	0.38	DZ-2	042/22SE	347/38	224/34	111/32	11
86-6	46°00′30″	6°41′22″	LDR	12	48	1.20	0.20	−1.40	15.58	0.20	DZ-3	264/14NW	101/79	218/06	308/12	1
87-1	45°53′09″	6°19′20″	LDR	12	48	0.37	−0.09	−0.28	27.08	0.08	DZ-3	047/55SE	004/57	109/08	202/30	0
87-3	45°54′10″	6°17′13″	LDR	12	48	0.89	0.16	−1.04	20.83	0.17	DZ-3	010/18E	184/49	357/38	095/08	11
87-4	45°54′22″	6°12′34″	LDR	12	48	0.68	0.09	−0.76	33.33	0.26	DZ-2	016/40SEO	017/33	110/01	198/56	41
			PEV	2	32	4.31	1.39	−5.69	9.38	0.93	DZ-2	016/40SEO	302/17	210/03	112/73	33
			NEV	1	25	1.10	−0.21	−0.89	8.00	0.27	DZ-2	016/40SEO	181/72	076/05	344/17	33
87-5	45°54′47″	6°11′55″	LDR	12	48	2.55	0.36	−2.91	12.50	0.44	DZ-2	340/44E	290/68	193/03	102/23	16
87-6	45°54′00″	6°09′58″	LDR	12	48	0.98	−0.25	−0.73	27.08	0.14	DZ-2	002/83EO	346/04	245/74	076/16	63
87-7	45°43′50″	6°05′47″	LDR	12	48	1.32	−0.59	−1.27	4.17	0.10	DZ-2	032/19E	035/04	298/54	128/35	17
87-8	45°47′44″	6°06′20″	LDR	12	48	1.10	0.61	−1.71	4.17	0.15	DZ-2	007/21E	000/50	198/37	103/10	11
87-9	45°54′26″	6°25′22″	LDR	12	48	0.83	0.47	−1.31	20.83	0.13	DZ-3	066/31SE	318/62	052/02	142/28	2
87-10	45°54′32″	6°25′13″	LDR	12	48	0.70	0.15	−0.85	16.67	0.13	DZ-3	063/43SE	354/07	099/67	260/23	28
87-11	45°53′01″	6°26′33″	LDR	12	48	0.23	0.02	−0.25	14.58	0.05	DZ-3	049/26NW	040/48	300/08	204/40	46
87-13	45°57′29″	6°18′58″	LDR	12	48	0.83	0.08	−0.91	10.42	0.08	DZ-3	065/25E	357/60	240/13	144/25	1
87-14	45°59′25″	6°16′03″	LDR	12	48	1.60	−0.44	−1.16	14.58	0.22	DZ-2	065/69W	168/10	262/10	032/78	14
87-15	46°02′07″	6°23′15″	LDR	12	48	1.53	−0.32	−1.21	12.50	0.31	DZ-3	10311SW	031/07	294/35	133/53	48
87-16	46°02′43″	6°22′47″	LDR	12	48	2.55	0.25	−2.80	25.00	0.30	DZ-2	060/88EO	051/23	231/68	321/00	80
87-17	45°59′02″	6°23′20″	LDR	12	48	2.32	0.60	−2.92	12.50	0.22	DZ-3	050/28E	060/86	318/00	228/04	3
87-18	46°03′23″	6°26′32″	LDR	12	48	0.41	0.15	−0.56	25.00	0.12	DZ-3	086/50N	090/54	229/29	330/20	25
87-19	46°02′37″	6°36′36″	LDR	12	48	0.64	0.00	−0.64	16.67	0.07	DZ-2	033/22E	136/43	013/30	262/32	45
87-20	45°58′55″	6°45′23″	LDR	12	48	4.99	−0.08	−4.91	33.33	1.77	AZ-5	053/09SE	035/40	176/43	287/20	27
			PEV	1	34	12.22	0.49	−12.71	0.00	2.01	AZ-5	053/09SE	049/24	198/64	314/11	20
			NEV	1	24	11.99	−2.48	−9.51	8.33	2.68	AZ-5	053/09SE	310/03	099/96	220/02	0
87-21	45°59′30″	6°45′12″	LDR	12	48	14.29	−5.53	−8.76	37.50	2.00	AZ-5	056/16SE	195/02	104/21	291/69	78
			PEV	2	36	19.56	−6.53	−13.03	8.33	2.01	AZ-5	056/16SE	192/05	104/09	314/80	84
			NEV	1	21	13.10	6.07	−19.17	9.52	3.11	AZ-5	056/16SE	058/87	294/02	204/03	7
87-22	46°02′37″	6°37′04″	LDR	12	48	2.72	−0.66	−2.06	16.67	0.22	DZ-2	015/11SE	206/13	103/44	310/41	51
87-23	46°03′26″	6°45′29″	LDR	12	48	4.99	−1.64	−3.35	37.50	0.66	DZ-4	150/34SW	011/33	258/30	137/42	40
			PEV	1	40	8.38	−2.24	−6.15	7.50	1.14	DZ-4	150/34SW	022/06	145/78	290/10	11
			NEV	1	19	3.78	1.44	−5.21	5.26	1.46	DZ-4	150/34SW	291/24	125/65	024/05	32
87-25	45°53′52″	6°11′16″	LDR	12	48	0.27	0.01	−0.28	8.33	0.04	DZ-2	163/38NE	355/07	258/48	092/42	6
87-26	46°02′01″	6°36′38″	LDR	12	48	0.77	0.45	−1.22	35.42	0.34	DZ-2	114/43NE	258/32	144/34	020/41	10
			PEV	2	27	7.16	−1.35	−5.81	7.41	1.32	DZ-2	114/43NE	061/12	153/08	276/76	50
			NEV	2	29	1.23	−0.32	−0.91	10.34	0.25	DZ-2	114/43NE	146/54	290/30	030/17	24
87-27	46°02′12″	6°37′18″	LDR	12	48	5.86	0.27	−6.13	14.58	0.73	DZ-2	027/27SE	092/24	199/32	333/46	64

problem will be restricted to the analysis of the exposed thrust sheet.

Previous workers have described transport indicators in the external Alps in and around the northern Subalpine Chain that suggest a dominant northwestward transport direction (Pijolat *et al.* 1981, Steck 1984, 1987, Choukroune *et al.* 1986, Platt *et al.* 1989, Vialon *et al.* 1989, Auborg *et al.* 1991) with a subsequent change to more westward displacement (Dietrich & Durney 1986, Gourlay 1986, Ramsay 1989, Huggenberger & Wildi 1991). The large-scale transport direction for the Jura was also to the northwest. The final model must be consistent with the northwestward large-scale transport direction.

Curvature models

Five models for curvature development (Fig. 1) have been quantified by Ferrill (1991a). The properties of these models are briefly reviewed before being tested against the field data. The predicted tangential (strike-parallel) and radial strains are emphasized because these have been determined for the northern Subalpine Chain.

Pure bending

Predicted pure bending strains for the northern Subalpine Chain curvature were calculated for three models, assuming no width change caused by the bending. The models differ in their position of the neutral surface: in model (a) the outer arc is neutral, in (b) the inner arc is neutral and in (c) an intermediate arc is neutral (Fig. 11). The placement of the marker lines in the models was chosen to approximate the orientations of the fold axes and to include the area of calcite twin strain data (Fig. 7). Calculated tangential strains (Fig. 1a) range from 0 to 57% shortening in the outer-arc-neutral model within the study area (Fig. 11a). Calculated tangential strains in the inner-arc-neutral model range from 21% shortening to 83% extension (Fig. 11b). The strains predicted in the intermediate-neutral-surface model range from 44% tangential contraction around the inner arc to 29% tangential extension around the outer arc (Fig. 11c). The large outer-arc extensions and/or inner-arc contractions, predicted by the pure bending model are not in accordance with the generally low calcite twin strains and the distribution of faults and associated tangential extension around the curvature. Therefore, the pure-bending model is not accepted for the curvature of the northern Subalpine Chain.

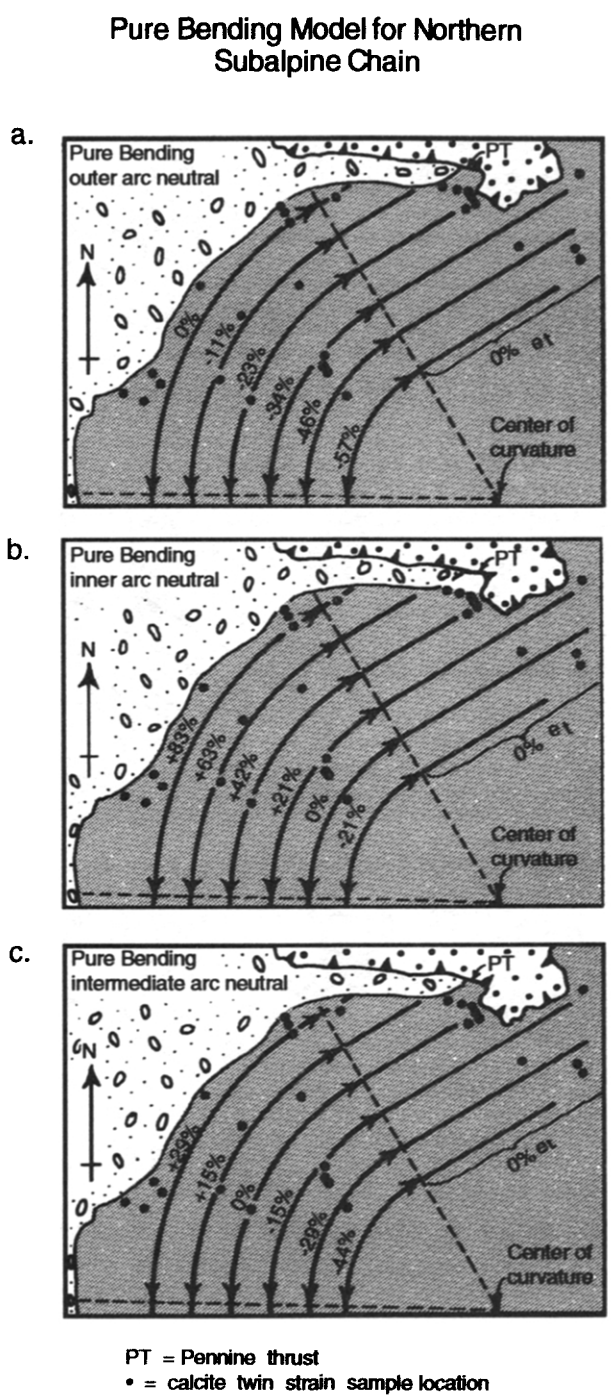

Fig. 11. Pure bending models for the northern Subalpine Chain. Dots represent locations of twin strain measurements. Tangential elongations are expressed as percentages: + = extension, − = contraction. (a) Outer-arc-neutral model predicts strike contractions ranging from 0% in the outer arc to 57% around the inner arc. (b) Inner-arc-neutral model predicts strike-parallel extensions ranging from 0% around the neutral arc to 83% around the outer arc. (c) Intermediate-arc-neutral model predicts strains ranging from 29% extension around the outer arc to 44% contraction around the inner arc. PT = Pennine thrust.

Radial thrusting

Tangential extensions for the radial thrusting model (Fig. 12) were calculated (Fig. 1b) using radial percent shortening values of 14, 22 and 25%, chosen for compatibility with shortening values measured from the northern Subalpine Chain cross-sections (Fig. 8). The most external continuous fold axis was used as the arc of no length change (B′ position in Fig. 8b). The fold-axis-parallel extensions increase towards the inner arc. The calculated strains around the curvature in the models are 0–26% extension (Fig. 12a), 0–59% extension (Fig. 12b), and 0–78% extension (Fig. 12c) for the models with 14, 22 and 25% curved-bed shortening in cross-section, respectively. The twin strain data and the distribution of cross-strike faults in the northern Subalpine

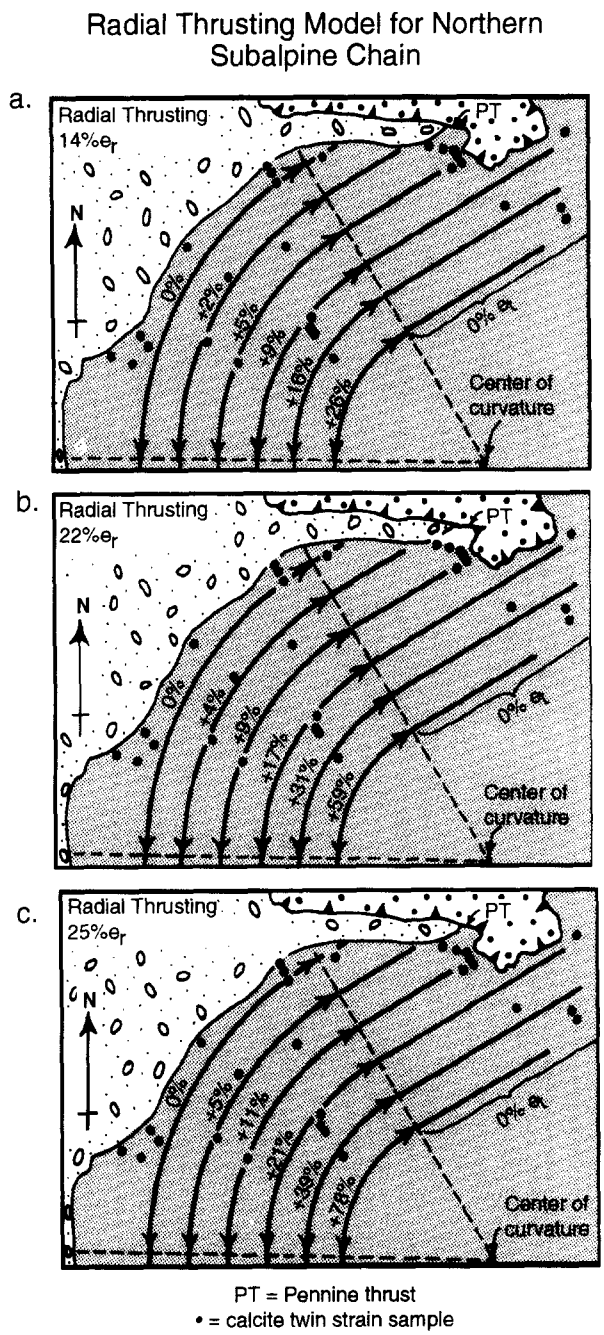

Fig. 12. Radial thrusting models for the northern Subalpine Chain. Dots represent locations of twin strain measurements. The outer arc is a surface of zero tangential strain. Tangential extensions (+) are given as percentages. Cross-strike shortenings of (a) 14, (b) 22 and (c) 25% are used in the models because they are the curved-bed values of shortening derived from the three cross-sections across the fold–thrust belt (Fig. 8). The tangential elongations predicted by the models are (a) 0–26%, (b) 0–59% and (c) 0–78%. PT = Pennine thrust.

Chain do not suggest the large tangential extensions around the inner arcs required by the radial thrusting model. Therefore, the radial thrusting model is not accepted for the northern Subalpine Chain curvature.

Curve-parallel simple shear

The curve-parallel simple shear model neither allows the strike extension by calcite twinning and map-scale faulting observed in the study area, nor explains the along-strike changes in the curved-bed cross-sectional shortening. Therefore, the model is not suitable for the northern Subalpine Chain curvature.

Uniform displacement–uniform shortening

The uniform displacement–uniform shortening model involves fold axes that are curved when they form and do not undergo tangential extension after their formation. The model cannot account for the strike extension by calcite twinning and map-scale faulting observed in the study area. Therefore, the model is not suitable for the northern Subalpine Chain curvature.

Transport-parallel simple shear

The transport-parallel simple shear model is applied to the northern Subalpine Chain based on a northwestward large-scale transport direction of 315° (Choukroune *et al.* 1986, Platt *et al.* 1989, Ramsay 1989, Vialon *et al.* 1989). In the model, displacement may be either variable or uniform in magnitude and conserved or consumed by shortening within the fold–thrust belt. If differential displacement is consumed, then the fold–thrust belt will have greater shortening at the center of the bend (Fig. 2c). For the northern Subalpine Chain, this should be manifested by more or tighter folds in the central domain. In the exposed Urgonian Limestone, this is not the case. Instead, the fold axes are for the most part continuous around the curvature (Moret 1934, Charollais *et al.* 1977, Ramsay 1989) and the radial shortening is less in the central domain (14%; Fig. 6) than in the other two domains (22 and 25%).

For uniform displacement differentially consumed, transport-parallel shortening gradually increases laterally away from the central region, and marker lines (fold axes) gradually approach each other farther away from the center (Fig. 2d). The radial shortening is greater in the northeastern and southern domains of the study area (similar to Fig. 3a) and the transition in shortening appears to be abrupt rather than gradual. In the southern domain, the fold axes abruptly become closer together and parallel to each other (Fig. 13) (Charollais *et al.* 1977) rather than gradually converging away from the central region as illustrated in Fig. 2(d). Version 1 of the model (differential displacement conserved; Figs. 2b and 3) is characterized by less radial shortening in the unrotated region and an abrupt increase in radial shortening in the rotated regions and it is here tested against the northern Subalpine Chain. The assumption of originally straight fold axes is made for the present modeling, but originally curved fold axes could also be modeled. Given the same final geometry, the tangential extension expected for originally curved axes that subsequently undergo transport-parallel simple shear is less than that for originally straight axes (Fig. 1e).

In the case of the northern Subalpine Chain, the transport-parallel shortening in the central domain (14%), which is assumed to be unrotated in map view, is used as the background shortening parallel to the large-

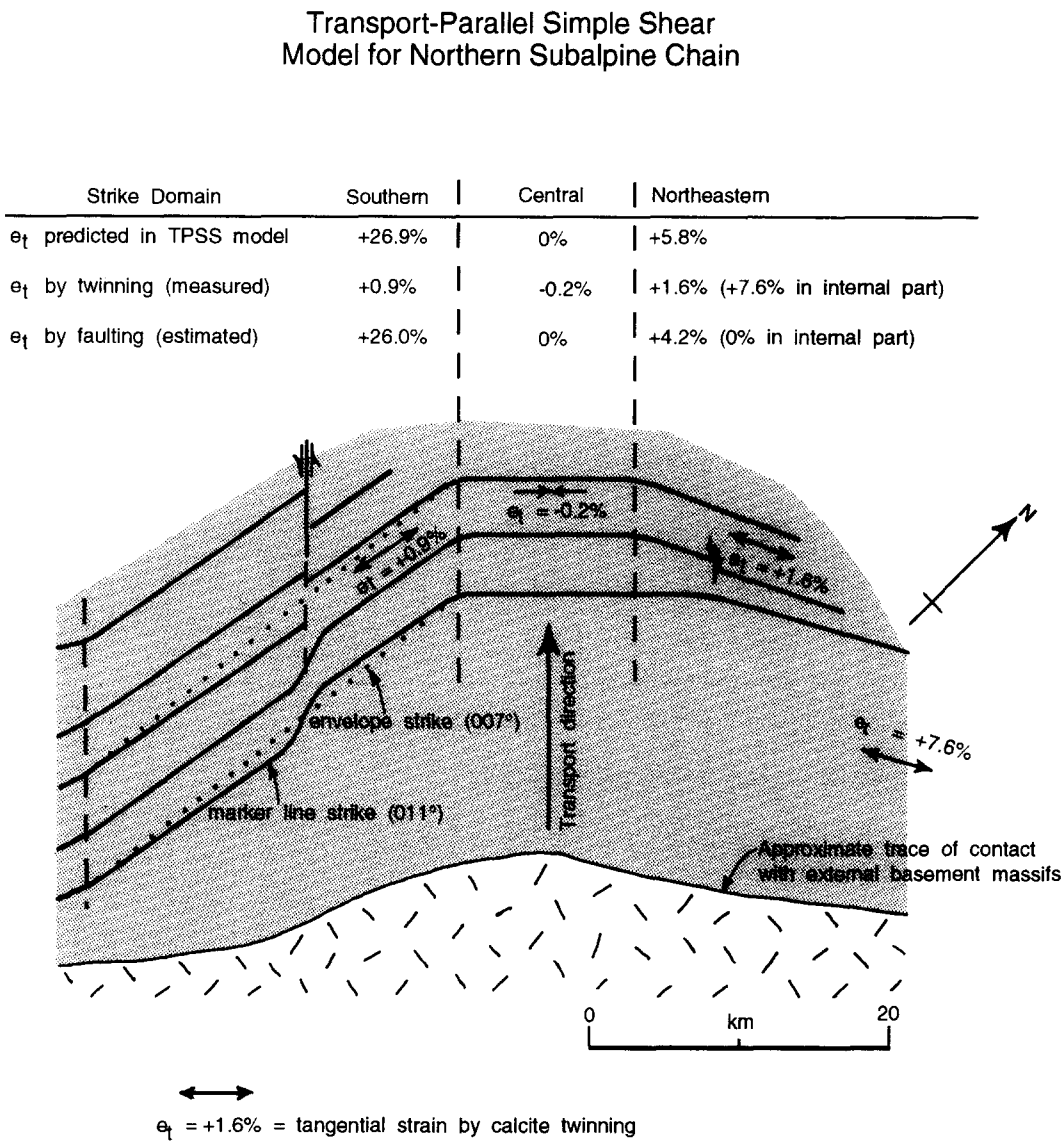

Fig. 13. Simplified map of the northern Subalpine Chain emphasizing the principal elements of the transport-parallel simple shear model. Estimated faulting strains were calculated, based on measured fault intensities, to make up the difference between the measured twinning strain and the predicted strain. Mapped fault separations are of the appropriate magnitudes for the estimated fault strains to be reasonable.

scale transport direction. The width of the unrotated part of the thrust sheet is, therefore, 86% of the original width. The radial width of the southern domain should be equal to 17.1% shortening (calculated using equation 1) of 86% of the original width, which is 71%, with a total apparent shortening of 29%. The curved-bed profile shortening measured from the southern domain cross-section (Fig. 8c) is 25%, only 4% less than the 29% predicted by the model, and, therefore, is a reasonably good fit. The rotation of 19° in the northeastern domain requires an additional 5.5% width reduction beyond the initial 14% shortening. The predicted total strike-normal shortening is, therefore, 19% for the northeastern zone. The measured curved-bed shortening for the zone is 22% (Fig. 8a), a difference of 3%. Again, there is reasonably good agreement between the measured radial shortening and the radial shortening predicted using the model.

Predicted tangential extensions are: 26.9% for the 38° rotation in the southern domain; 0% for the unrotated central region; and 5.8% for the 19° rotation in the northeastern domain (Fig. 13). The tangential extension is the total extension by mesoscopic and microscopic fracturing, faulting, ductile deformation, and by map-scale faulting.

The predicted 5.8% tangential elongation in the northeastern domain can be accounted for by internal strain and faulting. In the more internal parts of the northeastern domain, the average of 7.6% (LDR) tangential extension, recorded by twinning strain, more than accounts for the tangential extension predicted by this model. There is a general lack of cross-strike faults in the internal parts of the northeastern domain that would indicate additional tangential extension by faulting. The calcite twinning strains in the frontal parts of the northeastern domain record an average tangential extension of 1.6%, which leaves 4.2% extension to be accounted for by other mechanisms. As was discussed earlier, cross-strike faults are mapped and the displacements, where visible, generally have the appropriate

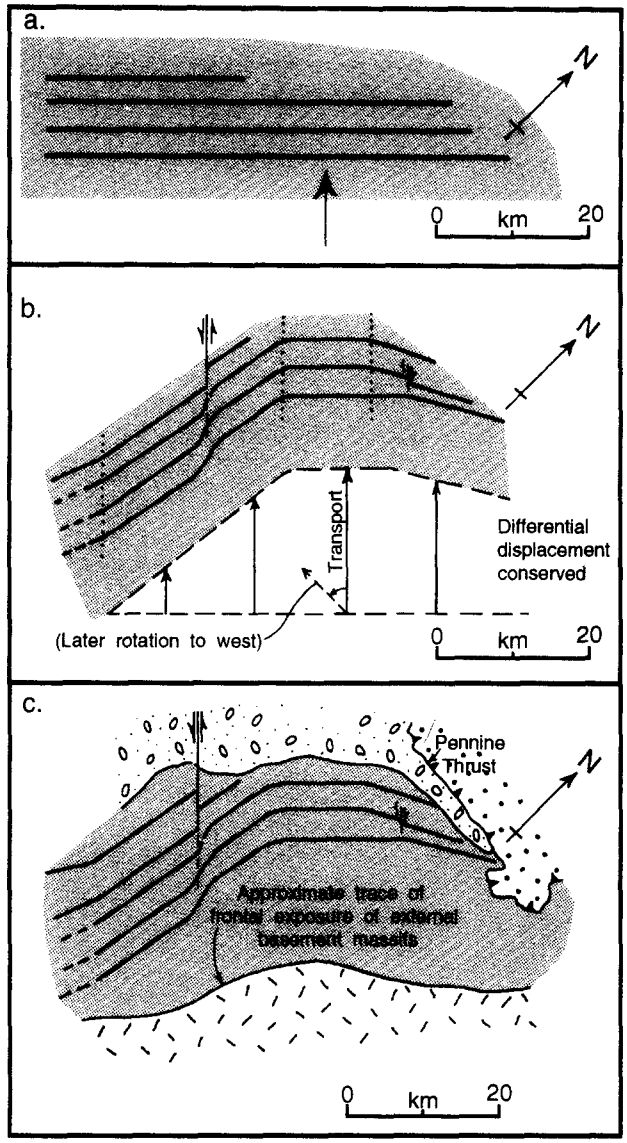

Fig. 14. Progressive development of the curvature in the northern Subalpine Chain, France. (a) Originally, NW-directed thrusting caused the bedding-parallel shortening strains (with e_3 axes parallel to the transport direction) and folding. (b) Differential displacement, still to the northwest, caused transport-parallel simple shear that rotated strike and caused passive rotation of the early formed strain axes, along-strike extension by faulting and continued twinning in limestone, and cross-strike shortening by fold tightening in the rotated regions. (c) Subsequently, the transport direction shifted to westward and locally caused calcite twinning and possible additional folding.

sense of separation to produce tangential extension as predicted in the model. The present fault intensity for the northern domain ranges from 1.9 to 4.6 faults km^{-1} parallel to strike, with an average of 3.3 faults km^{-1}. In general, the displacement magnitudes on the faults are not great enough to be measured from the 1:50,000 scale map. The 4.2% tangential extension that may be attributed to faulting amounts to 12.3 m of strike extension per fault for a fault spacing of 3.4 faults km^{-1} (spacing corrected for the 5.8% tangential extension predicted). Fault separations of the appropriate sense and apparent magnitude have been mapped (e.g. Fig. 9b) (Ricour *et al.* 1969, Charollais 1986). Huggenberger & Wildi (1991) measured 5% tangential extension by cross-strike normal faulting in the frontal part of the northeastern domain, which equals the tangential extension needed to account for the remaining strain predicted by the transport-parallel simple shear model.

The 38° strike rotation in the southern domain (Fig. 13) requires 26.9% tangential extension according to the transport-parallel simple shear model. The disparity between the trend of the fold axes (011°) and the envelope strike (007°) in the southern domain is related to the discontinuity of structures across the Vuache strike-slip fault that projects into the Subalpine Chain at Annecy (Fig. 5). This large fault strikes approximately parallel to the transport direction. After subtraction of the effect of this fault, a 20.6% extension along strike (4.97 km of the original 24.1 km length of the domain perpendicular to transport) remains to be accounted for. The microscopic plastic extension from the calcite twinning strain (0.9%) produces 217 m of tangential extension. Subtracting the tangential extension by twinning from the total predicted (4.97 km) leaves 4.75 km to be accounted for by other mechanisms. Tangential extension of 82.3 m per fault is needed (using the spacing of

2.0 faults km^{-1} corrected for 21% tangential extension to 2.4 faults km^{-1}) to account for the remaining tangential extension. Fault separations of the appropriate sense and apparent magnitude have been mapped (Fig. 7) (Goguel 1966). Part of the tangential extension attributed to map-scale faults may actually have occurred by mesoscopic extension fracturing and faulting. The fold axes in the southern domain may have originally formed slightly oblique to the large-scale transport direction. Originally curved fold axes would require less tangential extension in the southern domain and therefore would decrease the amount of tangential extension attributed to faulting and extension fracturing.

The transport-parallel simple shear model for the northern Subalpine Chain is supported by strike changes occurring across zones apparently parallel to the assumed regional transport direction (northwestward); width reductions of the fold-belt in rotated regions approximately equal to those predicted by the model; no tangential extension in the central domain where strike is perpendicular to the large-scale transport direction; and crystal-plastic strains and cross-strike faults in the southern and northeastern domains of the curvature appropriate to accommodate the tangential extension predicted by the model.

DISCUSSION

The differential displacement in the transport-parallel simple shear model for the northern Subalpine Chain does not require a rigid indenter as is commonly modeled (e.g. Laubscher 1972, Tapponnier & Molnar 1977, Vialon *et al.* 1984, Marshak 1988) but could simply be due to a difference in the accumulated displacement towards the foreland. Such a change in displacement magnitude could be caused by a lateral variation of shortening internal to the Subalpine Chain, as in the uniform-displacement differentially-consumed version of the transport-parallel simple shear model (Fig. 2d).

The transport-parallel simple shear model does not account for all the calcite twin strain shortening axes with azimuths between northwest and west. These data suggest a shift to westward transport. Such a transition from northwestward thrusting to westward thrusting was previously proposed for the northern Subalpine Chain by Ramsay (1989). Similarly, changing transport direction caused structural overprinting and discrete sets of transport indicators (e.g. slip lineations, stretching lineations, finite strain patterns) in the Helvetic Alps (Ramsay & Huber 1984, Dietrich & Durney 1986, Dietrich 1989, Dietrich & Casey 1989, Fry 1989a,b).

The interpreted change in transport direction could have been driven by either a change in the plate motion vector or changes caused by local body forces (Platt *et al.* 1989). A shift of short duration in the plate motion vector is not regionally recognized during or after folding of the Subalpine Chain (Platt *et al.* 1989). Instead, the shift of the transport direction to westward could have been caused by the local body forces. Mechanical modeling of tapering fold–thrust belts has illustrated that the shortening in a thrust wedge is partially controlled by the topographic slope (Davis *et al.* 1983, Dahlen 1990). Changes in the direction of topographic slope are expected as a curvature forms by the transport-parallel simple shear mechanism so that the slope direction becomes increasingly oblique to the transport direction as the curvature develops (Ferrill 1991a). The interpreted change in transport direction could have been driven by the local body forces caused by surface slopes oblique to the regional transport direction after the uplift and curvature of the Subalpine Chains had developed.

In summary, a model of transport-parallel simple shear in which differential displacement is conserved best approximates the structure and kinematics of the curvature of the northern Subalpine Chain. As mentioned earlier, the possibility exists that the fold axes in the southern domain of the curvature were originally somewhat curved and then rotated to their final configuration by transport-parallel simple shear, which would require less tangential strain than is predicted in the model for originally straight axes. However, the model based on the assumption of originally straight fold axes provides a good fit for the data.

Acknowledgements—We would like to thank Jean-Luc Epard, Patricia M. Kenyon, Peter Hudleston, Olivier Merle, O. Adrian Pfiffner, Harold H. Stowell and William A. Thomas for their helpful reviews of the manuscript. The Geological Society of America, the University of Alabama Student Government Association, ARCO, and the University of Alabama Graduate Council provided financial support for this research. Alastair Welbon is thanked for his support in the field. The version of the calcite strain gauge program by Mark Evans was most helpful for the strain analysis. This paper represents a portion of Ferrill's Ph.D. dissertation at the University of Alabama.

REFERENCES

Aprahamian, J. & Pairis, J.-L. 1981. Very low grade metamorphism with a reverse gradient induced by an overthrust in Haute-Savoie (France). In: *Thrust and Nappe Tectonics* (edited by McClay, K. R. & Price, N. J.). *Spec. Publs geol. Soc. Lond.* **9**, 159–165.

Auborg, C., Rochette, P. & Vialon, P. 1991. Subtle stretching lineation revealed by magnetic fabric of Callovian–Oxfordian black shales (French Alps). *Tectonophysics* **185**, 211–223.

Bayer, R., Cazes, M., Dal Piaz, G. V., Damotte, B., Elter, G., Gosso, G., Hirn, A., Lanza, R., Lombardo, B., Mugnier, J.-L., Nicolas, A., Nicolich, R., Polino, R., Roure, F., Sacchi, R., Scarascia, S., Tabacco, I., Tapponnier, P., Tardy, M., Taylor, M., Thouvenot, F., Torreilles, G. & Villien, A. 1987. Premiers résultats de la traversée des Alpes occidentales par sismique réflexion verticale (Programme ECORS-CROP). *C.r. Acad. Sci., Paris* **305**, 1461–1470.

Bonnet, J.-L. 1983. Etude du poinconnement d'une série stratifiée par le déplacement d'une écaille chevauchante. Exemples expérimentaux et naturels. Unpublished Ph.D. thesis, Université Scientifique et Médicale Grenoble.

Boyer, S. E. & Elliott, D. 1982. Thrust systems. *Bull. Am. Ass. Petrol. Geol.* **66**, 1196–1230.

Burkhard, M. 1990. Aspects of the large-scale Miocene deformation in the most external part of the Swiss Alps (Subalpine Molasse to Jura fold belt). *Eclog. geol. Helv.* **83**, 559–583.

Butler, R. W. H., Welbon, A., Gillcrist, R. & Coward, M. 1987. *External Western Alpine Thrust Belt*. Tectonic Studies Group Field-trip Guide.

Charollais, J. 1986. Carte Géologique de la France @ 1:50,000, feuille Annecy-Bonneville. Bureau des Recherches Geologiques et Minières, Orléans.

Charollais, J., Pairis, J.-L. & Rosset, J. 1977. Compte rendu de l'excursion de la Société Géologique Suisse en Haute-Savoie (France) du 10 au 12 octobre 1976. *Eclog. geol. Helv.* **70**, 253–285.

Choukroune, P., Ballèvre, M., Cobbold, P., Gautier, Y., Merle, O. & Vuichard, J.-P. 1986. Deformation and motion in the western Alpine arc. *Tectonics* **5**, 215–226.

Collet, L. W. 1927. *The Structure of the Alps*. Edward Arnold, London.

Coward, M. & Dietrich, D. 1989. Alpine tectonics—an overview. In: *Alpine Tectonics* (edited by Coward, M. P., Dietrich, D. & Park, R. G.). *Spec. Publs geol Soc. Lond.* **45**, 1–29.

Dahlen, F. A. 1990. Critical taper model of fold-and-thrust belts and accretionary wedges. *Annu. Rev. Earth & Planet Sci.* **18**, 55–99.

Davis, D., Suppe, J. & Dahlen, F. A. 1983. Mechanics of fold-and-thrust belts and accretionary wedges. *J. geophys. Res.* **88**, 1153–1172.

Debelmas, J. & Uselle, J.-P. 1966. La fin de la nappe de Morcles dans le massif du Haute-Giffre. *Bull. Soc. géol. Fr.* **8**, 337–343.

Dietrich, D. 1989. Fold-axis parallel extension in an arcuate fold-and-thrust belt: the case of the Helvetic nappes. *Tectonophysics* **170**, 183–212.

Dietrich, D. & Casey, M. 1989. A new tectonic model for the Helvetic nappes. In: *Alpine Tectonics* (edited by Coward, M.P., Dietrich, D. & Park, R. G.). *Spec. Publs geol. Soc. Lond.* **45**, 47–63.

Dietrich, D. & Durney, D. W. 1986. Change of direction of overthrust shear in the Helvetic nappes of western Switzerland. *J. Struct. Geol.* **8**, 389–398.

Dieterich, J. H. 1969. Origin of cleavage in folded rocks. *Am. J. Sci.* **267**, 155–165.

Dieterich, J. H. & Carter, N. L. 1969. Stress-history of folding. *Am. J. Sci.* **267**, 129–154.

Doudoux, B. 1973. Nouvelles données tectoniques sur le massif des Bauges (Savoie). *Ann. Centre Univ. Savoie* **1**, 125–139.

Dunne, W. M. & Ferrill, D. A. 1988. Blind thrust systems. *Geology* **16**, 33–36.

Epard, J.-L. 1990. La nappe de Morcles au sud-ouest du Mont-Blanc. *Mém. Géol. (Lausanne)* **8**.

Evans, M. A. & Dunne, W. M. 1991. Strain factorization and partitioning in a foreland thrust sheet. *J. Struct. Geol.* **13**, 21–35.

Ferrill, D. A. 1991a. Curvature development and limestone deformation in the northern Subalpine Chain (Haute-Savoie, France). Unpublished Ph.D. dissertation, University of Alabama.

Ferrill, D. A. 1991b. Calcite twin widths and intensities as metamorphic indicators in natural low-temperature deformation of limestone. *J. Struct. Geol.* **13**, 667–675.

Ferrill, D. A. & Groshong, R. H., Jr. In press. Deformation conditions in the northern Subalpine Chain, France, estimated from deformation modes in coarse-grained limestone. *J. Struct. Geol.*

Fry, N. 1989a. Short Paper: Kinematics of the Alpine Arc. *J. geol. Soc. Lond.* **146**, 891–892.

Fry, N. 1989b. Southwestward thrusting and tectonics of the western Alps. In: *Alpine Tectonics* (edited by Coward, M. P., Dietrich, D. & Park, R. G.). *Spec. Publs geol Soc. Lond.* **45**, 83–109.

Gehring, A. U., Keller, P. & Heller, F. 1991. Paleomagnetism and tectonics of the Jura arcuate mountain belt in France and Switzerland. *Tectonophysics* **186**, 269–278.

Goguel, M. J. 1966. Carte Géologique de la France @ 1:80,000, feuille Albertville. Bureau de Recherches Geologiques et Minières, Orléans.

Gourlay, P. 1986. La déformation du socle et des couvertures delphino-helvétiques dans la région du Mont Blanc (Alpes occidentales). *Bull. Soc. géol. Fr.* **8**, 159–169.

Groshong, R. H., Jr. 1972. Strain calculated from twinning in calcite. *Bull. geol. Soc. Am.* **83**, 853–862.

Groshong, R. H., Jr. 1974. Experimental test of the least-squares strain gauge calculation using twinned calcite. *Bull. geol. Soc. Am.* **85**, 1855–1864.

Groshong, R. H., Jr. 1975. Strain, fractures, and pressure solution in natural single-layer folds. *Bull. geol. Soc. Am.* **86**, 1363–1376.

Groshong, R. H., Jr. 1988. Low-temperature deformation mechanisms and their interpretation. *Bull. geol. Soc. Am.* **100**, 1329–1360.

Groshong, R. H., Jr., Pfiffner, O. A. & Pringle, L. R. 1984a. Strain partitioning in the Helvetic thrust belt of eastern Switzerland from the leading edge to the internal zone. *J. Struct. Geol.* **6**, 5–18.

Groshong, R. H. Jr., Teufel, L. W. & Gasteiger, C. 1984b. Precision and accuracy of the calcite strain-gage technique. *Bull. geol. Soc. Am.* **95**, 357–363.

Guellec, S., Tardy, M., Roure, F. & Mugnier, J.-L. 1989. Une interprétation tectonique nouvelle du massif Subalpin des Bornes (Alpes occidentales): apports des données de la géologie et de la géophysique profondes. *C.r. Acad. Sci., Paris* **309**, 913–920.

Huggenberger, P. & Wildi, W. 1991. La tectonique du massif des Bornes (Chaînes Subalpines, Haute-Savoie, France). *Eclog. geol. Helv.* **84**, 125–149.

Kübler, B., Martini, J. & Vuagnat, M. 1974. Very low grade metamorphism in the western Alps. *Schweiz miner. petrogr. Mitt.* **54**, 461–469.

Kübler, B., Pittion, J. L., Héroux, Y., Charollais, J. & Weidmann, M. 1979. Sur le pouvoir réflecteur de la vitrinite dans quelques roches du Jura, de la Molasse et des Nappes préalpines, hélvetiques, et penniques. *Eclog. geol. Helv.* **72**, 347–373.

Laubscher, H. P. 1972. Some overall aspects of Jura dynamics. *Am. J. Sci.* **272**, 293–304.

Marshak, S. 1988. Kinematics of orocline and arc formation in thin-skinned orogens. *Tectonics* **7**, 73–86.

Marshak, S., Geiser, P. A., Alvarez, W. & Engelder, T. 1982. Mesoscopic fault array of the northern Umbrian Apennine fold belt, Italy: Geometry of conjugate shear by pressure-solution slip. *Bull. geol. Soc. Am.* **93**, 1013–1022.

Matte, P. & Ribeiro, A. 1975. Forme et réorientation de l'ellipsoide de déformation dans la virgation hercynienne de Galice. Relations avec le plissement et hypothèses sur la genèse de l'arc ibéro-armorican. *C.r. Acad. Paris* **280**, 2825–2828.

Merle, O. 1989. Strain models within spreading nappes. *Tectonophysics* **165**, 57–71.

Moret, L. 1934. Géologie du massif des Bornes et des klippes préalpines des Annes et de Sulens (Haute-Savoie). *Mem. Soc. géol. Fr.* **22**, 1–162.

Mosar, J. 1988. Structures, déformation et métamorphisme dans les Préalpes Romandes (Suisse). Unpublished Ph.D. thesis, Université de Neuchatel, Neuchatel, Switzerland.

Mosar, J. 1989. Déformation interne dan les Préalpes medianes (Suisse). *Eclog. geol. Helv.* **82**, 765–793.

Mugnier, J.-L., Guellec, S., Ménard, G., Roure, F., Tardy, M. & Vialon, P. 1990. Crustal balanced cross-sections through the external Alps deduced from the ECORS profile. In: *Deep Structure of the Alps* (edited by Roure, F., Heizman, P. & Polino, R). *Mem. Soc. géol. Fr.* **156**.

Nicolas, A., Hirn, A., Nicolich, R., Polino, R. & ECORS-CROP Working Group 1990. Lithospheric wedging in the western Alps inferred from the ECORS-CROP traverse. *Geology* **18**, 587–590.

Pairis, B. 1975. Contributions à l'étude stratigraphique, tectonique et métamorphique du Massif de Platé (Haute-Savoie). Unpublished Ph.D. dissertation, Université Scientifique et Médicale de Grenoble, Grenoble, France.

Pairis, B. & Pairis, J.-L. 1978. Mécanismes de deformation dans le massif de Platé (Haute-Savoie). *Ann. Centre Univ. Savoie* **3**, 37–52.

Paréjas, E. 1925. La tectonique du Mont Joly (Haute-Savoie). *Eclog. geol. Helv.* **19**, 419–503.

Pfiffner, O. A. 1993. The structure of the Helvetic nappes and its relation to the mechanical stratigraphy. *J. Struct. Geol.* **15**, 511–521.

Pierce, W. G. 1966. Jura tectonics as a decollement. *Bull. geol. Soc. Am.* **77**, 1265–1276.

Pijolat, B., Gay, M., Gratier, J.-P. & Vialon, P. 1981. Les variations des valeurs de la déformation dans un système de plis par cisaillement. *Rev. Géol. Géogr. Phys.* **23**, 195–201.

Platt, J. P., Behrmann, J. H., Cunningham, P. C., Dewey, J. F., Helman, M., Parish, M., Shepley, M. G., Wallis, S. & Weston, P. J. 1989. Kinematics of the Alpine arc and the motion history of Adria. *Nature* **337**, 158–161.

Ramsay, J. G. 1967. *Folding and Fracturing of Rocks*. McGraw-Hill, New York.

Ramsay, J. G. 1989. Fold and fault geometry in the western Helvetic nappes of Switzerland and France and its implication for the evolution of the arc of the western Alps. In: *Alpine Tectonics* (edited by Coward, M. P., Dietrich, D. & Park, R. G.). *Spec. Publs geol. Soc. Lond.* **45**, 33–45.

Ramsay, J. G. & Huber, M. I. 1984. *The Techniques of Modern Structural Geology, Volume* 1: *Strain Analysis*. Academic Press, London.

Ricour, J., Rosset, J. & Schneegans, D. 1969. Carte Géologique de la France @ 1:80,000, feuille Annecy. Bureau de Recherches Geologiques et Minières, Orléans.

Ries, A. C. & Shackleton, R. M. 1976. Patterns and strain variations in arcuate fold belts. *Phil. Trans. R. Soc. Lond.* **A283**, 281–288.

Sanderson, D. J. 1982. Models of strain variation in nappes and thrust sheets: a review. *Tectonophysics* **88**, 201–233.

Schardt, H. 1898. Les régions exotiques du versant nord des Alpes suisses. *Bull Soc. Vaudoise Sci. Nat.* **34**, 113.

Spang, J. H. & Groshong, R. H., Jr. 1981. Deformation mechanisms and strain history of a minor fold from the Appalachian Valley and Ridge Province. *Tectonophysics* **72**, 323–342.

Spicher, A. 1980. Carte tectonique de la Suisse @ 1:500,000. Commission Geologique Suisse.

Steck, A. 1984. Structures de déformation tertiaires dans les Alpes centrales. *Eclog. geol. Helv.* **77**, 55–100.

Steck, A. 1987. Le massif de Simplon—Réflexions sur la cinématique des nappes de gneiss. *Schweiz mineral. petrogr. Mitt.* **67**, 27–45.

Tapponnier, P. & Molnar, P. 1977. Rigid plasic indentation: the origin of syntaxis in the Himalayan belt. *Coll. Int. Cent. Nat. Rech. Sci.* **268**, 431–432.

Teufel, L. W. 1980. Strain analysis of experimental superposed deformation using calcite twin lamellae. *Tectonophysics* **65**, 291–309.

Trümpy, R. 1980. *Geology of Switzerland, A Guidebook*. Ed. Schweiz. geol. Kommission 26, Wepf & Co., Basel.

Vialon, P., Bonnet, J.-L., Gamond, J.-F. & Mugnier, J.-L. 1984. Modélisation des déformations d'une série stratifiée par le déplacement horizontal d'un poiçon. Application au Jura. *Bull. Soc. géol. Fr.* **7**, 139–150.

Vialon, P., Rochette, P., & Ménard, G. 1989. Indentation and rotation in the western Alpine arc. In: *Alpine Tectonics* (edited by Coward, M. P., Dietrich, D. & Park, R. G.). *Spec. Publs geol. Soc. Lond.* **45**, 329–338.

Welbon, A. I. 1988a. Deformation styles and localization of thrust faults in the external French Alps. Unpublished Ph.D. dissertation, University of Leeds, U.K.

Welbon, A. I. 1988b. The role of intrabasinal faults on the development of a linked thrust system. *Geol Rdsch.* **77**, 11–24.

Zoetemeijer, R. & Sassi, W. 1992. 2-D reconstruction of thrust evolution using the fault-bend fold method. In: *Thrust Tectonics* (edited by McClay, K. R.). Chapman & Hall, London, 133–140.